TITLE: Resolving marine–freshwater transitions by diatoms through a fog of gene tree discordance and hemiplasy

RUNNING HEAD: Phylogenomics of marine and freshwater diatoms

AUTHORS:

Wade R. Roberts[1], Elizabeth C. Ruck[1], Kala M. Downey[1], Andrew J. Alverson[1,*]

[1]Department of Biological Sciences, University of Arkansas, 1 University of Arkansas, Fayetteville, AR, 72701, USA

[*]Corresponding author: Andrew J. Alverson, Department of Biological Sciences, University of Arkansas, 1 University of Arkansas, Fayetteville, AR, 72701, USA; aja@uark.edu

ABSTRACT

Despite the obstacles facing marine colonists, most lineages of aquatic organisms have colonized and diversified in freshwaters repeatedly. These transitions can trigger rapid morphological or physiological change and, on longer timescales, lead to increased rates of speciation. Diatoms are a lineage of ancestrally marine microalgae that have diversified throughout freshwater habitats worldwide. We generated a phylogenomic dataset of genomes and transcriptomes for 59 species to resolve freshwater transitions in one diatom lineage, the Thalassiosirales. Although most parts of the species tree were consistently resolved with strong support, we had difficulties resolving a Paleocene radiation, which affected the placement of one freshwater lineage. This and other parts of the tree were characterized by high levels of gene tree discordance caused by incomplete lineage sorting and low phylogenetic signal. Despite differences in species trees inferred from concatenation versus summary methods and codons versus amino acids, traditional methods of ancestral state reconstruction supported six transitions into freshwaters, two of which led to subsequent species diversification. However, simulations suggested as few as two independent transitions when accounting for hemiplasy, transitions occurring on branches in gene trees not shared with the species tree. This suggested that transitions across the salinity divide were originally facilitated by alleles already present in the ancestral marine populations. Accounting for differences in evolutionary outcomes, in which some taxa became locked into freshwaters while others were able to return to the ocean or become salinity generalists, might help distinguish between the ancestral changes that opened the door to freshwaters versus the subsequent, lineage-specific adaptations that allowed them to stay and thrive.

KEYWORDS: Gene concordance, Phylogenomics, Salinity, Site concordance, Thalassiosirales

INTRODUCTION

From bacteria to animals, the salinity gradient separating marine and freshwater environments poses a significant barrier to the distributions of many organisms (Lozupone and Knight 2007; McCairns and Bernatchez 2010; Kenny et al. 2019). Identifying how different lineages cross the salinity divide will improve our understanding of lineage diversification (Dittami et al. 2017) and the adaptive potential of species to climate change (Dickson et al. 2002; L E E et al. 2022). Diatoms are a diverse lineage of microalgae that occur throughout marine and freshwaters, and despite the numerous obstacles facing marine colonists (Kirst 1990, 1996; Nakov et al. 2020), ancestrally marine diatoms have successfully colonized and diversified in freshwaters repeatedly throughout their history (Nakov et al. 2019). These patterns are based on phylogenetic analyses of a small number of molecular markers, however, so they lack the insights of phylogenomic approaches, which can resolve large-scale macroevolutionary patterns and, at the same time, uncover key processes at play during important evolutionary transitions.

Although phylogenomic datasets have helped resolve historically recalcitrant nodes across the tree of life, they have also revealed how discordance in the evolutionary histories of different genes can confound inferences of species relationships. Gene tree discordance can be caused by biological sources, such as incomplete lineage sorting (ILS), hybridization, and compositional heterogeneity (Maddison 1997; Foster 2004; Degnan and Rosenberg 2006), or methodological sources, such as character sampling and gene tree error (Philippe et al. 2011; Xi et al. 2015; Molloy and Warnow 2018). Each of these challenge our ability to resolve species relationships and impact downstream analyses, such as estimation of divergence times (Smith et al. 2018). Multiple strategies have been proposed to overcome various sources of error, such as excluding third-codon positions from DNA datasets (Sanderson et al. 2000), using site-

heterogeneous models for amino acid data (Wang et al. 2018), and identifying the conditions under which concatenation (Edwards 2009) or gene tree summary approaches (Mirarab et al. 2014; Liu et al. 2015) more accurately resolve species relationships.

Discordance between gene and species trees can confound inferences of trait evolution as well (Hahn and Nakhleh 2016), particularly for complex traits that appear to have evolved convergently. Focusing on the species tree alone, without considering discordant gene trees, can lead to artifactual inferences of molecular convergence (Mendes et al. 2016). This failure occurs when a trait is determined by genes with topologies that do not match the species topology, a condition known as hemiplasy (Avise and Robinson 2008; Hahn and Nakhleh 2016; Storz 2016). Hemiplasy has been identified as a likely explanation for patterns of character incongruence in amino acid substitutions in columnar cacti (Copetti et al. 2017), flower and fruit traits in *Jaltomata* (Solanaceae) (Wu et al. 2018), and dietary specialization in *Dysdera* spiders (Vizueta et al. 2019). High levels of gene tree discordance were detected in all of these cases.

Adaptation to low salinity is a complex trait involving many genes and pathways (Jones et al. 2012; Artemov et al. 2017; Hughes et al. 2017; Paver et al. 2018), so the genomic changes associated with successful freshwater colonizations are multifaceted (Cabello-Yeves and Rodriguez-Valera 2019; Rogers et al. 2021) and generally involve mutations in multiple genes (DeFaveri et al. 2011; Terekhanova et al. 2019; Chen et al. 2021). To better understand the pattern, timing, and process of marine–freshwater transitions by diatoms, we assembled a dataset of 45 genomes and 42 transcriptomes—most of them newly sequenced—to resolve species relationships, explore the causes and consequences of gene tree discordance, and determine whether different freshwater transitions were influenced by hemiplasy.

MATERIALS & METHODS

Detailed methods are provided in Supplementary File S1. Briefly, fresh diatom cultures were isolated from natural plankton or acquired from the National Center for Marine Algae and Microbiota (NCMA) or Roscoff Culture Collection (RCC). Collection data, culture conditions, and voucher information are available in Supplementary Table S1. For genome and transcriptome sequencing, we extracted total DNA and RNA from diatom cultures, constructed sequencing libraries, and sequenced them on the Illumina platform. Based on a large multigene phylogeny of diatoms (Nakov et al. 2018), we included *Coscinodiscus,* Lithodesmiales, and *Eunotogramma* as outgroups. Accession numbers for reads and assemblies are provided in Supplementary Table S2.

We used OrthoFinder (Emms and Kelly 2019) to cluster amino acid sequences from all genomes and transcriptomes into orthogroups, then aligned orthogroups containing ≥20% of the taxa with MAFFT (Katoh and Standley 2013). For each alignment, we identified the best-fit substitution model using ModelFinder (Kalyaanamoorthy et al. 2017) and estimated gene trees with IQ-TREE (Minh et al. 2020b) or FastTree (Price et al. 2010). We then filtered and trimmed the gene trees using the Rooted Ingroup method to produce final ortholog sets (Yang and Smith 2014). This filtering and trimming procedure was performed twice. We used PAL2NAL (Suyama et al. 2006) to reconcile nucleotide coding sequence alignments against amino acid alignments. We used Degen (Regier et al. 2010; Zwick et al. 2012) to replace synonymous sites in the full coding sequence alignments with degenerate nucleotides. In total, we analyzed datasets consisting of amino acids (AA), the first and second codon positions (CDS12), and degenerate codons (DEGEN). We generated final ortholog alignments and inferred trees as described above, using 1000 ultrafast bootstrap replicates to estimate branch support (Minh et al.

2013). We generated summary statistics for the alignments and gene trees using AMAS (Borowiec 2016) and PhyKit (Steenwyk et al. 2021) (Supplementary Table S3). Correspondence analysis of amino acid frequencies across all taxa was performed using GCUA (McInerney 1998).

Species trees were inferred using maximum-likelihood analysis of a concatenated supermatrix with IQ-TREE and the summary quartet approach implemented in ASTRAL-III (Zhang et al. 2018). We performed the matched-pairs test of symmetry in IQ-TREE to identify and remove partitions that violated assumptions of stationarity, reversibility, and homogeneity (SRH; Naser-Khdour et al. 2019). For the IQ-TREE analysis, we partitioned supermatrices by gene, used ModelFinder to select the best-fit substitution model for each partition, and estimated branch support with 10,000 ultrafast bootstrap replicates. For ASTRAL, we used the ortholog trees as input, collapsing branches with low bootstrap support (<33) to help mitigate gene tree error (Sayyari and Mirarab 2016; Simmons and Gatesy 2021). We estimated branch support using local posterior probability (Sayyari and Mirarab 2016). In addition to heterogeneity in gene histories, substitutional heterogeneity can also make tree inference difficult at deep time scales (Lartillot and Philippe 2004). To account for this possibility, we also estimated a species tree from the concatenated amino acid matrix using the Posterior Mean Site Frequency (PMSF) model implemented in IQ-TREE (Wang et al. 2018).

We calculated the Robinson-Foulds distance between each pair of species trees and visualized the results with a multidimensional scaling plot made with the R package *treespace* (Jombart et al. 2017). We characterized discordance using gene and site concordance factors (Minh et al. 2020a) and quartet concordance factors (Pease et al. 2018). We tested the support for competing backbone topologies in our species tree using the approximately unbiased (AU) test

(Shimodaira 2002) implemented in IQ-TREE. Relative gene tree support for the same set of backbone topologies was further evaluated using gene genealogy interrogation method (Arcila et al. 2017). Finally, we performed the polytomy test on the ASTRAL species tree to test whether any of the unstable backbone branches were better represented as a polytomy (Sayyari and Mirarab 2018).

Divergence times were estimated using MCMCtree (Yang 2007; Reis and Yang 2011), using five fossil-based calibrations (Supplemental File S1), autocorrelated rates, and the approximate likelihood approach. We performed marginal ancestral state reconstruction for marine and freshwater habitat across the species tree using hidden state speciation and extinction (SSE) models in the R package *hisse* (Beaulieu and O'Meara 2016). Lastly, we explored the probability of hemiplasy in our habitat reconstructions using the models and approaches implemented in the R package *pepo* and the program HeIST (Guerrero and Hahn 2018; Hibbins et al. 2020). Due to the computational demands of gene tree simulations, HeIST simulations were based on a reduced 16-taxon tree.

Assembled genomes and transcriptomes have been deposited at NCBI under BioProject PRJNA825288. Predicted proteomes, phylogenomic datasets, and scripts have been deposited in the Dryad Digital Repository: _____.

RESULTS

We combined 42 newly sequenced draft genomes and 50 newly sequenced transcriptomes with publicly available genome or transcriptome data for a final dataset of 87 taxa representing 59 distinct species. A total of 17 transcriptomes were used directly in phylogenomic analyses, and the other 33 were used for genome annotation. From the combined dataset of

genomes and transcriptomes, we generated alignments and gene trees for 6262 orthologs, with each taxon represented in an average of 3275 (52.3%) orthologs.

Compositional heterogeneity and dataset construction

Relative Composition Variability (Phillips and Penny 2003) indicated greater compositional heterogeneity in third codon positions compared to amino acids and first and second codon positions (Supplementary Fig. S1). We also found substantial variation in GC content of third codon positions across taxa and genes (Supplementary Fig. S2), ranging from an average proportion of 0.40 ± 0.07 in *Cyclotella kingstonii* to 0.76 ± 0.14 in *Shionodiscus oestrupii*. To minimize potentially misleading signal in the nucleotide data, we removed third codon positions and, to examine the effects of saturation and GC heterogeneity in coding sequences (CDS), we replaced synonymous sites by recoding CDS sequences with degenerate nucleotides (Zwick et al. 2012). Based on these results, we created three datasets to estimate phylogenetic relationships: amino acids (AA), first and second codon positions (CDS12), and degenerate codons (DEGEN).

Dataset and alignment characteristics are summarized in Table 1 and detailed in Supplementary Table S3. Each dataset initially contained 6262 orthologs (Table 1). Gene trees constructed from all datasets were well supported (80 ± 7% average bootstrap; Supplementary Table S3). To reduce systematic errors due to model misspecification, we removed orthologs that failed assumptions of stationarity, reversibility, and homogeneity (SRH; $P < 0.05$), which retained 5522 (AA), 3259 (CDS12), and 3788 (DEGEN) loci in the datasets (hereafter referred to as the "complete" datasets; Table 1). We additionally subset the complete datasets to maximize signal or minimize missing data. To maximize signal and reduce stochastic error, we sorted

orthologs by the percentage of parsimony informative (PI) sites and retained the top 25% ranked orthologs ("top-PI"; Table 1). To minimize the amount of missing data and maximize taxon occupancy, we sorted complete datasets by the number of taxa and subset these to include the top 25% ranked orthologs with highest taxon occupancy ("top-Taxa"; Table 1). Orthologs in the top-Taxa datasets contained an average of 76 ± 8% of the total taxa.

Table 1. Summary of datasets used in the study.

Data type	Dataset name	Num loci	Total sites	Parsimony informative sites (%)	Num loci passing SRH[1]	*Thalassiosira* grade topology	
					$P < 0.05$	IQ-TREE	ASTRAL
Amino acids (AA)	complete	6262	3,777,062	60	5522	Topology 4	Topology 1
	top-PI	1588	996,027	76	1314	Topology 4	Topology 1
	top-Taxa	1574	808,477	64	1374	Topology 5	Topology 1
	top-PI-top-Taxa + PMSF[2] model	488	246,300	77	488	Topology 5	Topology 1
1st + 2nd codon positions (CDS12)	complete	6262	7,554,124	55	3259	Topology 4	Topology 5
	top-PI	1570	1,950,228	71	661	Topology 4	Topology 3
	top-Taxa	1574	1,616,954	59	782	Topology 5	Topology 3
Degenerate codons (DEGEN)	complete	6262	11,311,186	33	3788	Topology 4	Topology 3
	top-PI	1569	2,884,728	44	771	Topology 4	Topology 2
	top-Taxa	1574	2,425,431	36	903	Topology 5	Topology 3

[1] Matched-pairs test of Symmetry, Reversibility, and Homogeneity.

[2] Posterior Mean Site Frequency model.

Species tree inference and placement of freshwater clades

We initially estimated 18 species trees using amino acids, codon positions 1 and 2, and degenerate codon sequences with different cutoffs for taxon occupancy or proportion of parsimony informative sites, using both concatenation and summary quartet approaches (Table 1). Correspondence analysis of amino acid frequencies separated taxa principally by habitat (marine vs. freshwater) rather than phylogeny (Supplementary Fig. S3), which led us to explore whether substitutional heterogeneity affected phylogenetic reconstructions. To do so, we estimated an additional species tree using the PMSF mixture model, which can accommodate heterogeneity in the amino acid substitution process between sites (Wang et al. 2018). Due to the computational demands of implementing this model, we applied it only to a reduced amino acid dataset with orthologs that met both the top-PI and top-Taxa filtering criteria ("AA-top-PI-top-Taxa"; Table 1). Gene trees from this dataset were also used as input to ASTRAL.

Previous phylogenetic analyses resolved freshwater taxa into two main clades: the genus *Cyclotella*, which also includes several marine and brackish species, and the "cyclostephanoids", comprised of several stenohaline genera confined exclusively in freshwaters (Alverson et al. 2011). Given the potential implications for uncovering the mechanisms of freshwater adaptation, we were primarily interested in the placements of these two clades. Gross differences among data types and methods were evident in an ordination of species trees based on pairwise Robinson-Foulds distances, which showed a clear separation between IQ-TREE and ASTRAL topologies, with further separation of IQ-TREE trees estimated from datasets that maximized signal (top-PI) or minimized missing data (top-Taxa) (Supplementary Fig. S4). The phylogenetic position of *Cyclotella* was strongly supported and robust to differences in data type (codons vs. amino acids) and analysis (IQ-TREE vs. ASTRAL) (Fig. 1). The cyclostephanoids were placed

consistently within a large clade of marine *Thalassiosira* and relatives (Fig. 1), but the arrangements of five main subclades—*Thalassiosira* I–IV and the freshwater cyclostephanoids—varied depending on data type and analysis (Table 1; Fig. 2a). We refer to this part of the tree as the *Thalassiosira* grade.

One resolution of the *Thalassiosira* grade (topology 1), recovered only by ASTRAL analysis of amino acid gene trees, placed the freshwater cyclostephanoids as sister to a clade of *Thalassiosira* I–IV (Table 1; Fig. 2a). All other species trees placed cyclostephanoids as sister to *Thalassiosira* III (Table 1; Fig. 2a). ASTRAL analyses of codon-based gene trees (CDS12 and DEGEN) alone recovered topology 3, which placed cyclostephanoids and *Thalassiosira* III as sister to the remaining *Thalassiosira* (Table 1; Fig. 2a). Topologies 4 and 5 were recovered by both data types, but only topology 5 was robust to both data type and analysis, having been recovered by IQ-TREE analysis of both amino acid and codon alignments, and ASTRAL analysis of codon-based gene trees (Table 1; Fig. 2a). Moreover, topology 5 was also recovered by IQ-TREE analysis with the PMSF model, with almost all branches in the *Thalassiosira* grade receiving maximum support (Fig. 1, branches A–E). Notably, the PMSF analysis also recovered a monophyletic *Stephanodiscus*, which matches expectations based on morphology (Theriot et al. 1987). *Stephanodiscus* was paraphyletic, with strong support, in relation to *Cyclostephanos* in 18 of the 20 species trees. Based on all of these results, we chose topology 5 from the PMSF analysis as the reference species tree (Fig. 1).

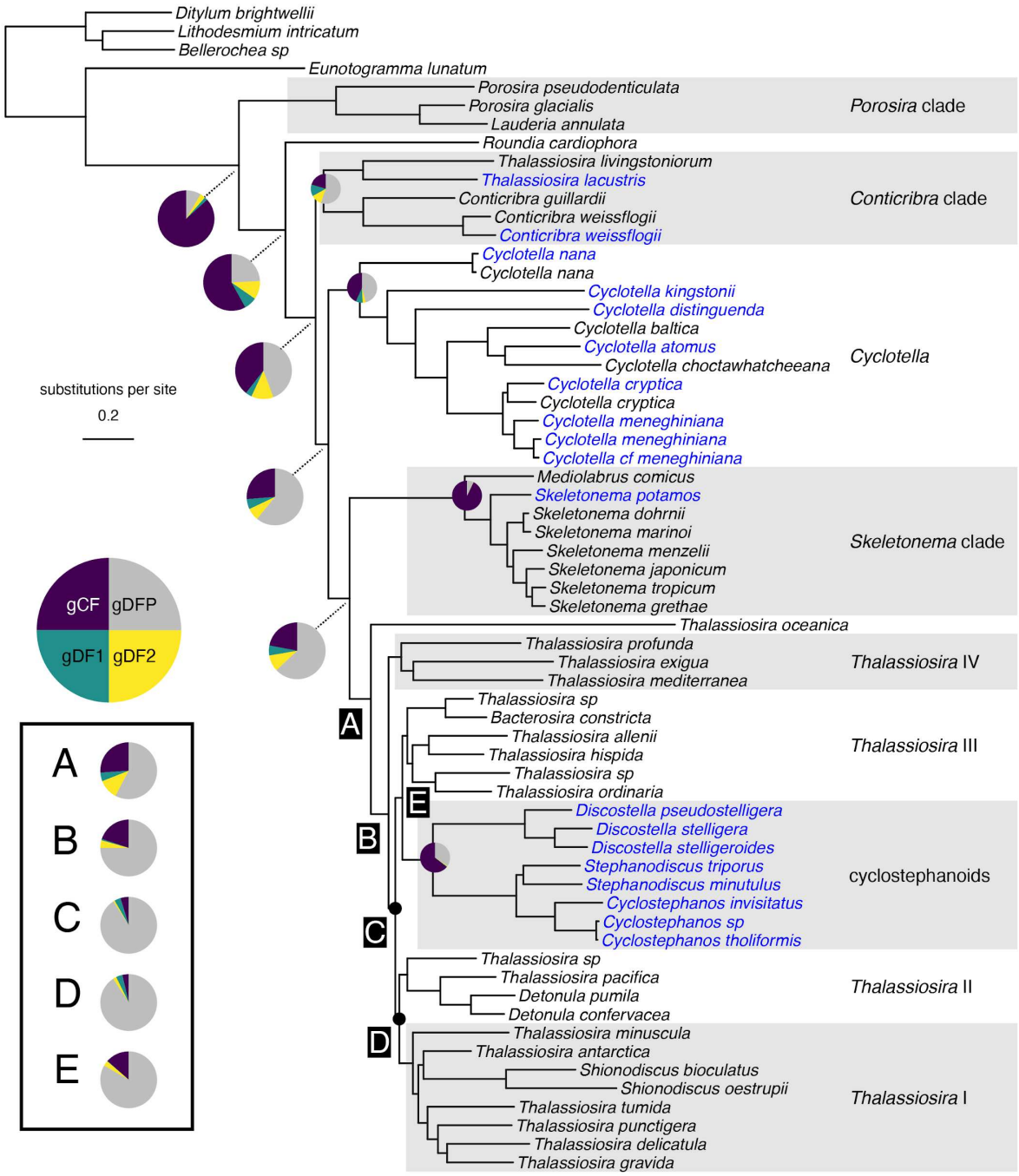

Figure 1. Phylogram based on maximum likelihood analysis of amino acids using the posterior mean site frequency (PMSF) model and a dataset of 488 loci with the highest proportions of taxa and informative sites ("AA-top-PI-top-Taxa" dataset; Table 1). Backbone nodes of the *Thalassiosira* grade are indicated by the letters A–E. All branches had bootstrap support (BS)

values of 100 except for those with black circles which had BS = 90. Pie charts on backbone nodes show the proportion of gene trees that support the clade (gCF), the proportion that support both discordant topologies (gDF1, gDF2), and the proportion that are discordant due to polyphyly (gDFP). The size of the pie charts is only for aesthetics.

Discordance underlies topological uncertainty

Discordance among genes and sites is an important factor impacting phylogenetic reconstruction (Degnan and Rosenberg 2006; Mallet et al. 2016) and multiple tools now exist for identifying and characterizing discordance (Salichos et al. 2014; Smith et al. 2015; Pease et al. 2018). We characterized discordance by calculating gene, site, and quartet concordance factors for each branch (Figs. 1 and 2a; Supplementary Figs. S5 and S6). Gene (gCF) and site concordance factors (sCF) represent the proportion of genes or sites that are in agreement with a particular branch in the species tree (Minh et al. 2020a). Gene concordance factors range from 0 to 100, and site concordance factors typically range from one-third (33) to 100, with values near 33 indicative of no signal for that branch (Minh et al. 2020a). Quartet concordance factors (QC) provide an alternative, likelihood-based estimate of the relative support at each branch for the three possible resolutions of four taxa (Pease et al. 2018). Quartet concordance factors range from -1 to 1, with positive values showing support for the focal branch, negative values supportive for an alternate quartet, and values of zero indicating equal support among the three possible quartets (Pease et al. 2018).

All three concordance factors were high for most branches in the tree, indicating that a majority of genes, sites, and quartets supported those relationships (Supplementary Figs. S5 and S6). For example, the branch subtending the *Skeletonema* clade had high concordance

(gCF/sCF/QC = 93/75/0.87; Supplementary Figs. S5 and S6). Despite having maximum bootstrap and local posterior probability support, however, concordance factors were low for many of the backbone branches (Fig. 1; Supplementary Figs. S5 and S6). These included backbone branches within the *Thalassiosira* grade (Fig. 1, nodes A–E) that affected placement of the freshwater cyclostephanoids (Fig. 2). In this part of the tree, concordance was generally low for the backbone branches (gCF = 4–26; sCF = 32–42; QC = –0.04–0.36) (Figs. 1 and 2; Supplementary Figs. S5 and S6). Gene concordance factors were lowest for branches C and D, the only two branches in the species tree with <100% bootstrap support (Fig. 1). Gene concordance factors were only slightly higher for branches A, B, and E (Fig. 1). These had low site concordance (Fig. 2a) and near-zero quartet concordance factors (Supplementary Fig. S6), consistent with expectations for little to no signal. Site concordance factors did not change appreciably when we used the CDS12 data. However, repeating quartet concordance factor calculation with the CDS12 data revealed a minor switch in support for branches C ($QC_C = 0.004 \rightarrow -0.006$) and E ($QC_E = -0.04 \rightarrow 0.07$) (Supplementary Fig. S6). These patterns of shifting support combined with the lowest site concordance factor for branch E ($sCF_E = 32$) suggest that very few sites support the sister relationship of *Thalassiosira* III and cyclostephanoids, despite its recovery in 16 of the 20 inferred species trees (Figs. 1 and 2a).

Although bootstrap and posterior probability values were uniformly high across our trees, traditional measures of branch support often fail to capture the underlying agreement or disagreement among genes or sites for a given tree topology (Minh et al. 2020a). For many of the branches on our tree, there were more discordant than concordant genes and sites (Fig. 1; Supplementary Figs. S5 and S6), suggesting that more genes and sites supported an alternative relationship. This was the case with *Stephanodiscus*, for example, where more genes supported

paraphyly than monophyly, though more sites supported monophyly (Supplementary Figs. S5 and S6). Across the tree, support for alternative relationships was neither strong nor consistent among genes or sites. Illustrative of this, discordance in more than one-third of the tree (29 of 83 branches) was due to polyphyly (Supplementary Fig. S5), indicative of a widespread lack of signal in our gene trees. Taken together, these analyses highlighted extensive gene and site discordance, some well-supported and much of it not, across Thalassiosirales.

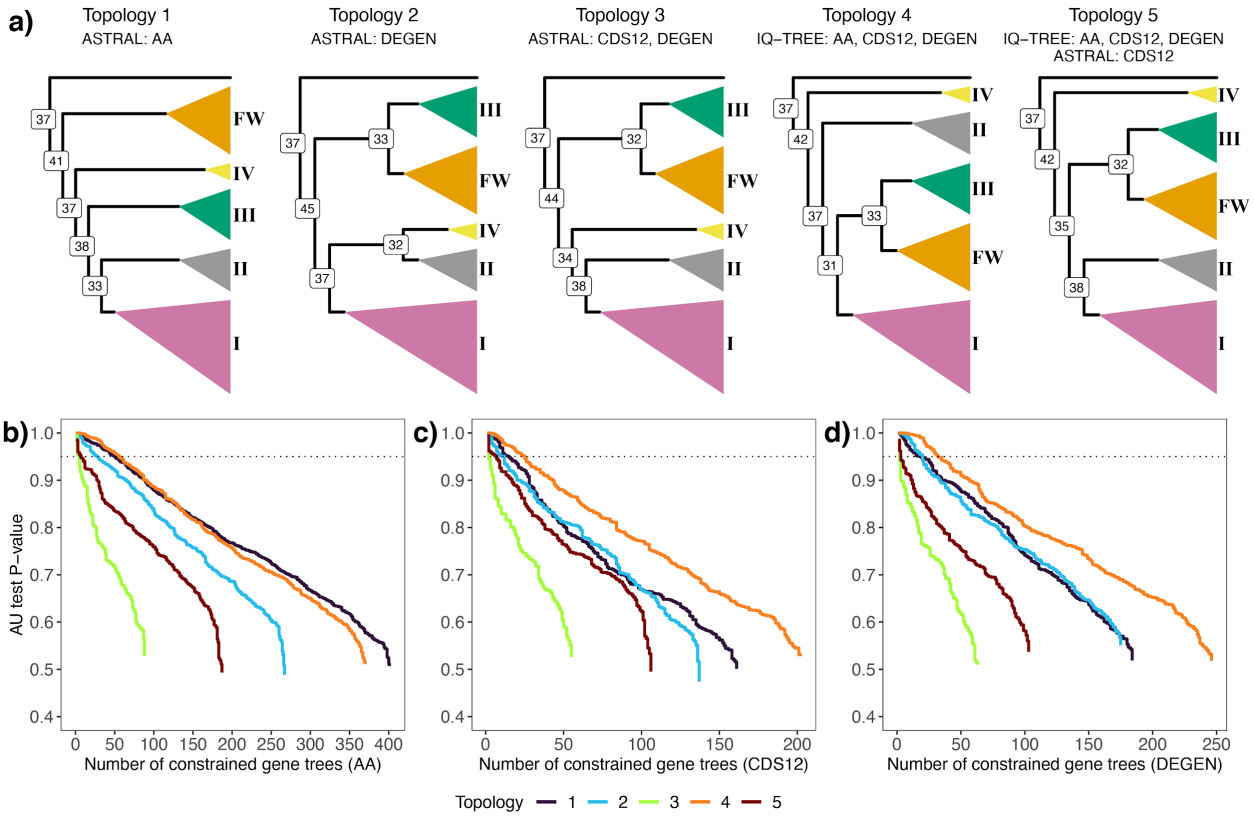

Figure 2. **a)** Phylogenetic hypotheses of the *Thalassiosira* grade inferred using concatenation and summary methods on the amino acid (AA), codon positions 1 and 2 (CDS12), and recoded codon (DEGEN) datasets. Nodes are labeled with the percentage of amino acid sites concordant with the branch (site concordance factor). The principal clade of interest, the freshwater cyclostephanoids, is colored orange and labeled 'FW'. The four focal clades of marine

303 *Thalassiosira* and allies are labeled I–IV. Below, results of gene genealogy interrogation tests of
304 alternative hypotheses of relationships within the *Thalassiosira* grade. These tests used datasets
305 filtered to include only the top 25% of orthologs based on the percentage of parsimony
306 informative sites (top-PI) for **b)** amino acids, **c)** codon positions 1 and 2, and **d)** recoded codons.
307 Lines correspond to the cumulative number of genes (x-axis) supporting topology hypotheses
308 with the highest probability and their *P* values (y-axis) from the Approximately Unbiased (AU)
309 topology tests. Values above the dashed line indicate topological hypotheses that are
310 significantly better than the alternatives ($P < 0.05$). For example, the green line in (b) shows that
311 there were a total of 88 genes that best supported topology 3, while only four of those genes were
312 above the dotted line and were significantly better supported than the other four alternative
313 topologies.
314
315 There are both biological (e.g., ILS) and technical causes (e.g., gene tree error) of gene
316 discordance, but the proportion attributable to each factor can be difficult to discern (Morales-
317 Briones et al. 2020; Cai et al. 2021). To better assess the importance of gene tree error in our
318 dataset—whether genes with low phylogenetic signal produced inaccurate gene trees—we
319 recalculated gene and site concordance using just the 1588 amino acid orthologs with the highest
320 percentage of parsimony informative sites (top-PI dataset; Table 1). Average gene concordance
321 increased modestly, from 56.6% to 62.1%, but site concordance was unchanged (Supplemental
322 Fig. S7). Gene concordance factors for branches A, B, and E in the *Thalassiosira* grade increased
323 by 5–7% but were largely unchanged for branches C and D (Supplemental Fig. S7). These
324 increases in gene concordance when using the most signal-rich genes suggest that errors in gene
325 tree estimation contributed to the lack of resolution in several critical branches (Chan et al. 2020;

Vanderpool et al. 2020). Deeper nodes in the tree may be more prone to technical errors caused by long-branch attraction, poor alignments, or model misspecification, despite our attempts to minimize these during dataset construction (Supplementary File S1). We found slight negative correlations between node age and both gene concordance ($R^2 = 0.10$) and site concordance ($R^2 = 0.26$) (Supplementary Fig. S8), which suggests that older branches more likely suffered from saturation due to recurrent substitutions.

Placement of the freshwater cyclostephanoids

We used two additional tree-based methods to test the relative support for competing topologies within the *Thalassiosira* grade. Approximately unbiased (AU) tests on the concatenated alignment for each dataset in Table 1 were used to assess the relative statistical support for topologies 1–5 (Fig 2a). Like the original species tree inferences, results of AU tests largely reflected data type (Table 1), with amino acid characters supporting topology 1 ($P = 0.01$, AU test) and the codon and degenerate codon datasets supporting topology 4 ($P = 0$, AU test; Supplementary Table S4). Although concordance factors suggested that most gene trees were uninformative for relationships in the *Thalassiosira* grade, we looked for secondary signal for one or more of the five competing topologies using gene genealogy interrogation (GGI; Arcila et al. 2017). To do this, we performed constrained gene tree searches on the most information-rich (top-PI) orthologs and compared their likelihoods using the AU test. The GGI test assumes monophyly of the tested clades, so using our time-calibrated tree, we converted branch lengths (in millions of years) to coalescent time units using a range of plausible effective population sizes and generation times for diatoms (Supplementary File S1). The estimated stem branch lengths for the five clades in the *Thalassiosira* grade were all >5 coalescent units, suggesting

sufficient time to reach monophyly (Rosenberg 2003). After ranking likelihood scores from the AU tests and selecting constraint topologies with the best score (rank 1 trees), no single topology was strongly favored in a majority of constrained gene trees across the three datasets, implying similar levels of support (Fig. 2b–d; Supplementary Table S5). Support from the amino acid dataset was split between topologies 1 and 4, which were recovered by both summary and concatenation methods (Table 1; Fig. 2b; Supplementary Table S5). The most frequent best-fit topology for the codon and degenerate codon datasets corresponded to topology 4 (Fig. 2c,d), one originally recovered by concatenation only (Table 1).

Gene genealogy interrogation can also be used to explore the effects of gene tree error on summary quartet methods by filtering the input to ASTRAL to include only the highest ranking constrained genes (Arcila et al. 2017; Mirarab 2017). For each of the three character types, we performed two ASTRAL analyses using as input either all the top scoring (rank 1) constrained gene trees ($n_{AA} = 1588$, $n_{CDS12} = 1570$, $n_{DEGEN} = 1569$) or just the subset that had statistical support ($P < 0.05$) above the AU-based rank 2 topology ($n_{AA} = 142$, $n_{CDS12} = 56$, $n_{DEGEN} = 71$). In all six cases, the inferred trees were consistent with topology 5, despite it being best supported (rank 1) in just 13–16% of the constrained gene trees (Fig. 2b–d; Supplementary Table S5). We originally chose topology 5 as the reference species tree (Fig. 1) because it was recovered by both amino acids and codons, ASTRAL and IQ-TREE analysis with the PMSF model, and because it recovered monophyly of *Stephanodiscus*. Coalescent theory predicts that in severe cases of ILS, short internal branches can produce gene trees that conflict with the species tree more often than they agree, creating the so-called “anomaly zone” (Degnan and Rosenberg 2006). Our recovery of a species tree topology here that is not the most frequent among the GGI gene trees could indicate that the backbone of the *Thalassiosira* grade lies in the anomaly zone.

Despite this, polytomy tests in ASTRAL using each dataset rejected the null hypothesis that any of these branches is a polytomy ($P < 0.05$).

The temporal sequence of marine–freshwater transitions

Divergence time estimates dated the crown Thalassiosirales to the upper Cretaceous, around 113 Ma (96–120, 95% CI; Fig. 3a; Supplementary Fig. S9). One of the two main freshwater lineages, *Cyclotella*, originated in the late Cretaceous (79 Ma [66–86, 95% CI]) and the other freshwater lineage, the cyclostephanoids, originated later in the Eocene (43.5 Ma [36–48, 95% CI]) (Fig. 3a; Supplementary Fig. S9). Radiation of the *Thalassiosira* grade lineages occurred during the Paleocene, from 57 Ma [48–63, 95% CI] to 73 Ma [61–80, 95% CI] (Fig. 3a; Supplementary Fig. S9). The overlapping confidence intervals allow for the possibility that these lineages diverged in much more rapid succession than suggested by the mean ages.

Hemiplasy impacts marine–freshwater transitions

We estimated the number of marine–freshwater transitions in two ways. A traditional trait reconstruction method, HiSSE, was used to estimate the maximum number of independent marine–freshwater transitions under a "homoplasy-only" model. A second model allowed us to estimate how many of the transitions were non-independent due to hemiplasy, i.e., transitions to freshwater occurring on branches of discordant gene trees that are not found in the species tree (Hibbins et al. 2020). The best-fit HiSSE model was a character independent model (CID-4, AIC = 535.3; Supplementary Table S6), which suggests that shifts in diversification rate occurred independently of marine–freshwater transitions. Using parameter estimates from the CID-4 model, we inferred six transitions from marine to freshwater habitats (Fig. 2a). With this dataset,

395 the most recent common ancestor of *Cyclotella* was marine, with the transition to freshwater
396 occurring shortly thereafter (Fig. 2a). To assess the possible role of hemiplasy in our trait
397 reconstructions, we calculated hemiplasy risk factors (HRF), which are the ratio of the
398 probabilities of hemiplasy to homoplasy in different parts of the species tree (Guerrero and Hahn
399 2018). This analysis revealed an increased chance of character state transitions due to hemiplasy
400 along most of the backbone branches of the species tree (Fig. 3b). Gene trees simulated from a
401 reduced 16-taxon species tree using HeIST returned 1133 loci with a simulated site pattern that
402 matched the marine–freshwater character states (i.e. freshwater taxa shared the same mutation).
403 With this approach, the most likely scenario is the one supported by the largest number of gene
404 trees. In our dataset, the scenarios could range from strict homoplasy (n = 6 marine–freshwater
405 transitions) to strict hemiplasy (n = 1 transition). A total of 732 of the 1133 simulated gene trees
406 (64.6%) corresponded to a scenario of combined hemiplasy and homoplasy, with two
407 independent transitions into freshwaters (Supplementary Table S7). Under this model, freshwater
408 taxa grouped into one of two clades in a simulated gene tree—each clade representing a
409 freshwater transition—where at least one transition was discordant with the species tree. Just
410 23% of the simulated trees supported a hemiplasy-only model with a single freshwater transition,
411 and there was no support for a homoplasy-only history of six independent marine–freshwater
412 transitions (Supplementary Table S7).
413

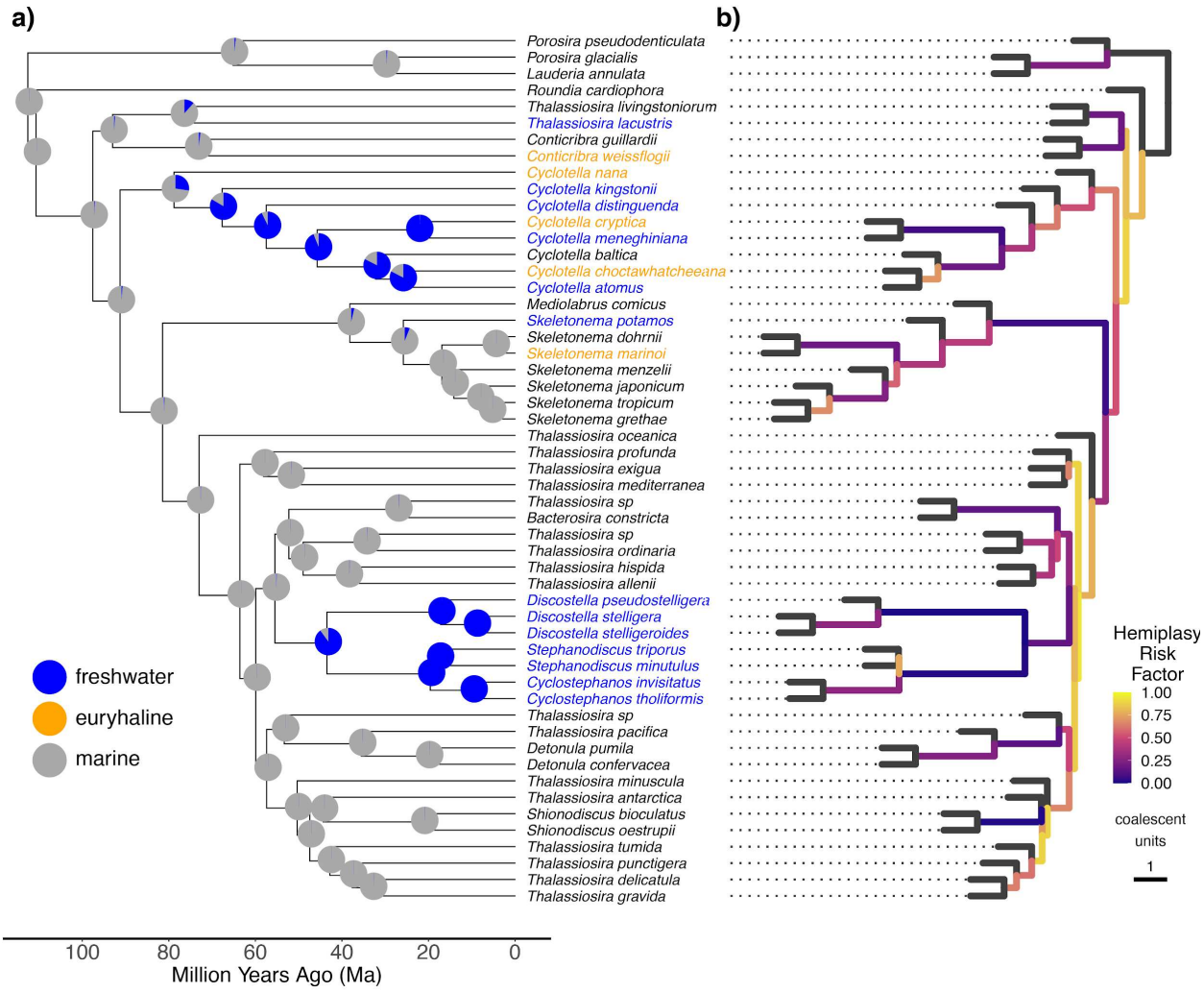

Figure 3. **a)** Divergence times and ancestral state reconstruction of marine and freshwater habitat in the Thalassiosirales. Conspecific taxa were removed prior to ancestral state reconstruction, leaving one tip per species. Tip labels are colored according to their habitat (blue=freshwater, orange=euryhaline, grey=marine). Pie charts denote the probability of each node reconstructed as either marine (grey) or freshwater (blue) using parameters estimated from the HiSSE CID–4 model. Euryhaline taxa were coded as marine for the purposes of ancestral state reconstruction. Divergence times for the full set of taxa can be found in Supplementary Fig. S9. **b)** Hemiplasy Risk Factors (HRF) on internal branches show increased values on most short internal branches,

demonstrating an increased potential for hemiplasy to influence trait reconstruction. Branch lengths in coalescent units were inferred using ASTRAL.

DISCUSSION

Transitions to freshwaters

Marine–freshwater transitions have been key events in the diversification of lineages across the tree of life (Logares et al. 2009; e.g., Tedesco et al. 2017), including diatoms where freshwater taxa have experienced significantly increased rates of both speciation and extinction compared to their marine ancestors (Nakov et al. 2019). Our study focused on one model clade, the Thalassiosirales, which is among the most abundant and diverse lineages in the marine and freshwater plankton and where genetic and genomic resources are readily available (Armbrust et al. 2004; Nawaly et al. 2020; Roberts et al. 2020). The 42 draft genomes presented here greatly expand the phylogenetic and ecological diversity of sequenced genomes for Thalassiosirales, and diatoms as a whole, and will greatly facilitate efforts to identify the genomic basis of freshwater adaptation in diatoms.

We identified six different marine–freshwater transitions in Thalassiosirales, more than previous studies (Alverson et al. 2007). We tested whether these transitions were fully independent, owing to separate mutations (homoplasy) in each of the six freshwater lineages, or whether some of the transitions were attributable to hemiplasy, i.e., shared ancestral polymorphisms in discordant gene trees (Avise and Robinson 2008). Hemiplasy simulations supported a scenario of as few as two independent transitions at the genic level, a result that followed naturally from the extensive history of gene tree discordance across the backbone of the tree. Long considered an ecological “Rubicon” that is rarely crossed (Mann 1999), phylogenetic

studies have shown that diatoms move much more frequently across the salinity divide than was assumed historically (Alverson et al. 2007; Nakov et al. 2019). The discovery of hemiplasy, which reduced the number of independent freshwater transitions in Thalassiosirales by a factor of three, suggests that transitions across steep environmental gradients might occur more commonly than expected when colonists can leverage ancestral polymorphisms rather than relying exclusively on new mutations.

With hundreds of species, a crown age of roughly 100 Mya, and freshwater transitions dating as far back as 80 Mya, the breadth and depth of the Thalassiosirales phylogeny far exceeds other, much younger lineages with traits that have been impacted by hemiplasy (Copetti et al. 2017; Wu et al. 2018). Relatively deep, and short, backbone branches that predated freshwater transitions were the ones identified as most susceptible to hemiplasy. The coalescent branch lengths were short in these parts of the tree (Fig. 3b), and the substitution- (Fig. 1) and clock-based branch lengths (Fig. 3a) are also shorter than suggested by our trees due to incomplete taxon sampling (Alverson et al. 2007). Although many of the conditions for hemiplasy were clear (high levels of gene tree discordance coinciding with a rapid radiation, particularly along the *Thalassiosira* grade), other properties of the habitat transitions were indicative of homoplasy: ancestral state reconstructions were unambiguous, the two main freshwater transitions were not paraphyletic but were aligned with phylogenetic relationships, and gene concordance was high on the long internal branches subtending the two main freshwater lineages (Hahn and Nakhleh 2016; Wu et al. 2018).

Given the sheer length of time that has elapsed since the transitions occurred, the shared ancestral polymorphisms that opened the door to freshwaters for Thalassiosirales will be difficult to distinguish from the augmenting, lineage-specific adaptive mutations that followed (Zou and

Zhang 2015; Mendes et al. 2016). A large number of genes and pathways have been implicated in the response to low salinity (Nakov et al. 2020; Downey et al. 2022; Pinseel et al. 2022), so an adaptive allele in one of the many possible target genes might have made it possible simply to survive in freshwaters initially. In the tens of millions of years since then, the hemiplasious alleles could have been overwritten in one or more freshwater lineages, leaving the shared mechanism itself (e.g., enhanced transport of sodium ions) as the only remaining direct evidence of the hemiplasy. The divergent evolutionary outcomes might also help distinguish hemiplasy from homoplasy. The genus *Cyclotella* includes freshwater, secondarily marine, and generalist euryhaline species that can tolerate a wide range of salinities (Guillard and Ryther 1962; Nakov et al. 2020; Downey et al. 2022). Similarly, most freshwater transitions at the tips of the tree (Fig. 1) involved species with populations that also grow in marine habitats (*Conticribra weissflogii* and *Cyclotella nana*) or can tolerate slightly brackish water (*Thalassiosira lacustris* and *Skeletonema potamos*). The cyclostephanoids are, by contrast, stenohaline specialists found exclusively in freshwaters, suggestive of a different genetic trajectory into freshwaters.

Although we have treated salinity as a categorical variable, salinity varies along a continuum from freshwater to marine and even hypersaline habitats. Moreover, salinity fluctuations are common in brackish and marine systems, such as coastlines influenced by precipitation and river discharge. Adaptation to variable environmental conditions may be more likely linked to modifications of gene expression (Wray 2007). In diatoms, exposure to freshwater induces profound changes gene expression related to cellular metabolism, ion transport, photosynthesis, and storage compound biosynthesis (Bussard et al. 2017; Nakov et al. 2020; Downey et al. 2022; Pinseel et al. 2022). Diatoms exhibit high levels of inter- and intraspecific variation in gene expression in response to reduced salinity (Nakov et al. 2020;

Pinseel et al. 2022), providing numerous targets for natural selection to optimize gene expression for a particular salinity environment (López-Maury et al. 2008; Bedford and Hartl 2009; Gomez-Mestre and Jovani 2013). Finally, differences in codon usage (Prabha et al. 2017), nucleotide substitution rates (Mitterboeck et al. 2016), transposable element activity (Yuan et al. 2018), epigenetic responses (Artemov et al. 2017), and epistatic interactions (Stern et al. 2022) have been implicated in adaptation to freshwaters in other groups. The genomic resources and phylogenetic framework presented here represent an important advance towards identifying the genes and evolutionary processes underpinning freshwater adaptation by diatoms.

The impact of discordance on placement of freshwater clades

Comparative analyses require a strong phylogenetic framework (Felsenstein 1985), so a major goal of this study was to establish a robust phylogenetic hypothesis for Thalassiosirales. Our primarily genome-based analysis of 6262 nuclear orthologs provided better resolution and, superficially, increased support across most of the tree compared to previous analyses based on a few genes (Alverson et al. 2007). Across character types, methods of inference, and different criteria for including characters or taxa, the placement of one of the two principal freshwater clades, *Cyclotella*, was consistent across species trees, with an estimated origin in the late Cretaceous. The placement of the second major freshwater lineage, the cyclostephanoids, was less certain.

The freshwater cyclostephanoid clade was placed within a grade of marine species, most of which belong to the polyphyletic genus *Thalassiosira*. These marine *Thalassiosira* were divided among four clades, but the arrangement of these clades and the freshwater cyclostephanoids varied across analyses. Uncertainty in the backbone relationships for this part

of the tree was likely caused by a combination of gene tree error and high levels of incomplete lineage sorting. First, many individual genes contained too little information to confidently resolve deep splits separated by short branch lengths—a finding that is not unique to this dataset (Chan et al. 2020; Arcila et al. 2021). Divergence time estimates suggest that these splits occurred in relatively quick succession, as few as 5 million years. Although many of these bipartitions had consistently weak support, gene concordance factors increased when we analyzed orthologs with the highest phylogenetic signal, implicating gene tree error as one of the sources of instability (Chan et al. 2020; Vanderpool et al. 2020). In other phylogenomic studies impacted by low phylogenetic signal and high gene tree error, gene genealogy interrogation (GGI) has been used to overcome noise and identify majority gene support for a single hypothesis (Hughes et al. 2018; Tea et al. 2021). In our case, no single resolution was supported by a majority of genes, indicative of nodes that are difficult to resolve even with hundreds of genes (Nesi et al. 2021). The best-supported constraint tree identified by GGI differed between amino acid and codon-based gene trees, highlighting conflicting signal even within genes. Second, in addition to gene tree error, the large number of alternative topologies among gene trees along the *Thalassiosira* grade is also consistent with ILS (Arcila et al. 2017). Gene tree summary methods such as ASTRAL outperform concatenation when ILS is the major source of discordance (Kubatko and Degnan 2007; Roch and Warnow 2015), but summary methods perform poorly when gene tree error is high (Roch and Warnow 2015; Xi et al. 2015). Following Arcila et al. (2017), we attempted to eliminate some of the noise in our dataset by restricting ASTRAL analyses to the top-ranked constrained gene trees and in doing so recovered a backbone topology congruent with one of the few originally recovered by both gene tree summary and concatenation methods (topology 5; Table 1 and Fig. 2). Taken together, these

538 results suggest that gene tree error negatively impacted our ASTRAL analyses. After identifying
539 and removing some of that error, we were able to recover a stronger hypothesis for the placement
540 of the freshwater cyclostephanoids within the marine *Thalassiosira* grade.

541 The anomaly zone describes an especially vexing phylogenetic problem in which short
542 branch lengths are unresolvable, resulting in gene trees that differ from the species more
543 frequently than they agree (Degnan and Rosenberg 2006). Within the *Thalassiosira* grade, the
544 most common GGI gene tree topologies either did not match the reference species tree or were
545 uninformative for these short branches. This implies that unresolved gene trees (i.e., those with
546 polytomies) are more probable than resolved ones in the *Thalassiosira* grade, as branch lengths
547 that exceed the boundaries of the anomaly zone should produce resolved gene trees (Huang and
548 Knowles 2009). Gene tree error like that identified in our dataset can lead to underestimation of
549 coalescent branch lengths, which define the anomaly zone boundaries (Linkem et al. 2016;
550 Forthman et al. 2022), resulting in the mistaken identification of an anomaly zone where none
551 exists. Although not entirely clear in our case, the *Thalassiosira* grade appears to fall outside of
552 the anomaly zone, so the large number of conflicting gene histories is more likely due to ILS and
553 gene tree error. Challenges remain in anomaly zone detection due to the limited application and
554 computational costs of multispecies coalescent methods applied to large genomic datasets and
555 the inclusion of additional biological factors other than ILS (Flouri et al. 2018, 2020).

556 Factors that are more poorly known in diatoms might also have contributed to the high
557 levels of discordance. We attempted to minimize technical sources of gene tree error during
558 dataset construction (Supplemental File S1), but other sources are more difficult to discern (Cai
559 et al. 2021). These include hybridization and polyploidy, gene duplication and loss, or
560 recombination. Although hybridization is not well documented in diatoms (Casteleyn et al. 2009;

561 Koester et al. 2010; Tanaka et al. 2015), there is evidence for an ancient allopolyploidy event
562 early on in the evolutionary history of Thalassiosirales (Parks et al. 2018). Many methods that
563 identify hybridization based on gene trees (Edelman et al. 2019; Vanderpool et al. 2020) or site
564 patterns in an alignment (Blischak et al. 2018) can be confounded by ancestral population
565 structure, substitutional saturation, or unsampled ghost lineages (Slatkin and Pollack 2008;
566 Tricou et al. 2022), all of which are poorly characterized in diatoms. High GC content regions
567 have been linked to higher recombination rates (Kent et al. 2012; Lartillot 2013) and can lead to
568 increased discordance (Pease and Hahn 2013). Despite high levels of variation in GC content
569 across Thalassiosirales, intralocus recombination was detected in a vanishingly small (<0.001%)
570 percent of the 6262 orthologs in our analysis (results available on Dryad). In addition to showing
571 whether any of these factors contribute to gene tree discordance, a more thorough exploration of
572 each one will fill important gaps in our understanding of diatom evolution.
573
574 *Codon bias and amino acid composition in freshwater diatoms*
575 Thalassiosirales includes divergence times across a timescale ranging from thousands
576 (Theriot et al. 2006) to tens of millions of years ago (Fig. 3a), which led us to explore the utility
577 of both amino acid and nucleotide characters for resolving phylogenetic relationships. Amino
578 acids are less susceptible to saturation and useful for resolving deep relationships (Philippe et al.
579 2011; Rota-Stabelli et al. 2012), whereas nucleotides contain more information to resolve more
580 recent divergences (Simmons et al. 2002; Townsend et al. 2008). Both data types recovered the
581 vast majority of relationships consistently and with strong support, while at the same time
582 revealing similar patterns of discordance along the backbone of the tree. In many cases, however,
583 they differed in their resolutions of the most recalcitrant parts of the tree. Disagreements between

584 character types within the same dataset, such as those within the *Thalassiosira* grade here, have
585 been found in other groups as well (Gillung et al. 2018; Skinner et al. 2020).

586 Almost every analysis of the amino acid dataset—including species trees, concordance
587 factors, and AU tests—supported the placement of cyclostephanoids as sister to the remaining
588 *Thalassiosira* clades, but nucleotide analyses placed them with *Thalassiosira* III (Fig. 2).
589 Discordance caused by codon usage bias and differences in amino acid composition might
590 account for this discrepancy. An association between codon bias and ecology has been
591 demonstrated in a broad diversity of microbes, where species that share an ecological niche have
592 similar codon usage, independent of phylogeny (Botzman and Margalit 2011; Roller et al. 2013;
593 Arella et al. 2021). Similar patterns of codon usage within marine and freshwater habitats have
594 been described in prokaryotes (Cabello-Yeves and Rodriguez-Valera 2019), and we discovered
595 differences in both codon usage and amino acid composition between marine and freshwater
596 diatoms. The amino acid compositions of distantly related freshwater lineages might be
597 sufficiently similar to cause the amino acid characters to support the "sister to the rest"
598 placement of cyclostephanoids. Protein sites with different structural, functional, or selective
599 constraints can lead to differences in amino acid composition between species (Villar and
600 Kauvar 1994; Youssef et al. 2021), something that is not accounted for by standard empirical
601 protein models and may have led to artifacts in our gene and species tree inferences (Wang et al.
602 2018). When we applied the PMSF model, which accounts for substitution heterogeneity in
603 amino acid sites, cyclostephanoids were placed as sister to *Thalassiosira* III, in agreement with
604 the codon datasets. The similarity in codon usage and amino acid composition between distantly
605 related freshwater diatoms merits further study into the causes and functional significance, if
606 any.

607

608 *Conclusions*

609 The vast differences between marine and freshwaters result in strong selective pressures
610 on freshwater colonists. Indeed, some of these transitions have become some of our most
611 powerful model systems for studying convergent evolution (Elmer and Meyer 2011). Low
612 salinity provokes a broad range of physiological and metabolic responses in diatoms (Nakov et
613 al. 2020; Downey et al. 2022; Pinseel et al. 2022), but the current genetic architectures of
614 freshwater adaptation reflect tens of millions of years of optimization and change since the
615 earliest transitions. As a result, it may not be possible to distinguish the derived alleles that
616 currently allow these diatoms to thrive in freshwaters from the ancestral ones that made the first
617 transitions possible. Nevertheless, the phylogenomic analyses presented here highlighted a key
618 role for hemiplasy in charting the genetic trajectory for freshwater colonizations in this group of
619 diatoms, indicating that some of the necessary alleles were already present in the ancestral
620 marine populations. Some of the subsequent mutations that built upon this scaffold of hemiplasy
621 might be identifiable by the different evolutionary outcomes in which some taxa became
622 irreversibly locked into freshwaters (e.g., cyclostephanoids) while others were able to transition
623 back to the ocean or became salinity generalists (e.g., *Cyclotella*). The vast new genomic
624 resources and phylogenetic framework presented here represent an important step forward in
625 addressing these types of questions to better understand how diatoms have made this complex
626 ecological transition appear to be so simple superficially.

627

SUPPLEMENTAL MATERIAL

Datasets and scripts are available from the Dryad Digital Repository: http://dx.doi.org/10.5061/dryad.[NNNN]

FUNDING

This work was supported by the National Science Foundation (DEB 1651087 to A.J.A). This research used resources available through the Arkansas High Performance Computing Center, which is funded through multiple NSF grants and the Arkansas Economic Development Commission.

ACKNOWLEDGEMENTS

We thank Ed Theriot for sharing several culture strains, and we thank Matt Ashworth and Jeffery Stone for help with scanning electron microscopy.

642 LITERATURE CITED

643 Alverson A.J., Beszteri B., Julius M.L., Theriot E.C. 2011. The model marine diatom
644 *Thalassiosira pseudonana* likely descended from a freshwater ancestor in the genus
645 Cyclotella. BMC Evol. Biol. 11:125.

646 Alverson A.J., Jansen R.K., Theriot E.C. 2007. Bridging the Rubicon: Phylogenetic analysis
647 reveals repeated colonizations of marine and fresh waters by thalassiosiroid diatoms. Mol.
648 Phylogenet. Evol. 45:193–210.

649 Arcila D., Hughes L.C., Meléndez-Vazquez B., Baldwin C.C., White W.T., Carpenter K.E.,
650 Williams J.T., Santos M.D., Pogonoski J.J., Miya M., Ortí G., Betancur-R R. 2021. Testing
651 the Utility of Alternative Metrics of Branch Support to Address the Ancient Evolutionary
652 Radiation of Tunas, Stromateoids, and Allies (Teleostei: Pelagiaria). Syst. Biol. 70:1123–
653 1144.

654 Arcila D., Ortí G., Vari R., Armbruster J.W., Stiassny M.L.J., Ko K.D., Sabaj M.H., Lundberg J.,
655 Revell L.J., Betancur-R. R. 2017. Genome-wide interrogation advances resolution of
656 recalcitrant groups in the tree of life. Nature Ecology & Evolution. 1:1–10.

657 Arella D., Dilucca M., Giansanti A. 2021. Codon usage bias and environmental adaptation in
658 microbial organisms. Mol. Genet. Genomics. 296:751–762.

659 Armbrust E.V., Berges J.A., Bowler C., Green B.R., Martinez D., Putnam N.H., Zhou S., Allen
660 A.E., Apt K.E., Bechner M., Brzezinski M.A., Chaal B.K., Chiovitti A., Davis A.K.,
661 Demarest M.S., Detter J.C., Glavina T., Goodstein D., Hadi M.Z., Hellsten U., Hildebrand
662 M., Jenkins B.D., Jurka J., Kapitonov V.V., Kröger N., Lau W.W.Y., Lane T.W., Larimer

663 F.W., Lippmeier J.C., Lucas S., Medina M., Montsant A., Obornik M., Parker M.S., Palenik
664 B., Pazour G.J., Richardson P.M., Rynearson T.A., Saito M.A., Schwartz D.C.,
665 Thamatrakoln K., Valentin K., Vardi A., Wilkerson F.P., Rokhsar D.S. 2004. The genome
666 of the diatom *Thalassiosira pseudonana*: Ecology, evolution, and metabolism. Science.
667 306:79–86.

668 Artemov A.V., Mugue N.S., Rastorguev S.M., Zhenilo S., Mazur A.M., Tsygankova S.V.,
669 Boulygina E.S., Kaplun D., Nedoluzhko A.V., Medvedeva Y.A., Prokhortchouk E.B. 2017.
670 Genome-Wide DNA Methylation Profiling Reveals Epigenetic Adaptation of Stickleback to
671 Marine and Freshwater Conditions. Mol. Biol. Evol. 34:2203–2213.

672 Avise J.C., Robinson T.J. 2008. Hemiplasy: A new term in the lexicon of phylogenetics. Syst.
673 Biol. 57:503–507.

674 Beaulieu J.M., O'Meara B.C. 2016. Detecting Hidden Diversification Shifts in Models of Trait-
675 Dependent Speciation and Extinction. Syst. Biol. 65:583–601.

676 Bedford T., Hartl D.L. 2009. Optimization of gene expression by natural selection. Proc. Natl.
677 Acad. Sci. U. S. A. 106:1133–1138.

678 Blischak P.D., Chifman J., Wolfe A.D., Kubatko L.S. 2018. HyDe: A Python Package for
679 Genome-Scale Hybridization Detection. Syst. Biol. 67:821–829.

680 Borowiec M.L. 2016. AMAS: a fast tool for alignment manipulation and computing of summary
681 statistics. PeerJ. 4:e1660.

682 Botzman M., Margalit H. 2011. Variation in global codon usage bias among prokaryotic

683 organisms is associated with their lifestyles. Genome Biol. 12:R109.

684 Bussard A., Corre E., Hubas C., Duvernois-Berthet E., Le Corguillé G., Jourdren L., Coulpier F.,
685 Claquin P., Lopez P.J. 2017. Physiological adjustments and transcriptome reprogramming
686 are involved in the acclimation to salinity gradients in diatoms. Environ. Microbiol. 19:909–
687 925.

688 Cabello-Yeves P.J., Rodriguez-Valera F. 2019. Marine-freshwater prokaryotic transitions require
689 extensive changes in the predicted proteome. Microbiome. 7:117.

690 Cai L., Xi Z., Lemmon E.M., Lemmon A.R., Mast A., Buddenhagen C.E., Liu L., Davis C.C.
691 2021. The Perfect Storm: Gene Tree Estimation Error, Incomplete Lineage Sorting, and
692 Ancient Gene Flow Explain the Most Recalcitrant Ancient Angiosperm Clade,
693 Malpighiales. Syst. Biol. 70:491–507.

694 Casteleyn G., Adams N.G., Vanormelingen P., Debeer A.-E., Sabbe K., Vyverman W. 2009.
695 Natural hybrids in the marine diatom *Pseudo-nitzschia pungens* (Bacillariophyceae):
696 genetic and morphological evidence. Protist. 160:343–354.

697 Chan K.O., Hutter C.R., Wood P.L. Jr, Grismer L.L., Brown R.M. 2020. Target-capture
698 phylogenomics provide insights on gene and species tree discordances in Old World
699 treefrogs (Anura: Rhacophoridae). Proc. Biol. Sci. 287:20202102.

700 Chen M.-Y., Teng W.-K., Zhao L., Hu C.-X., Zhou Y.-K., Han B.-P., Song L.-R., Shu W.-S.
701 2021. Comparative genomics reveals insights into cyanobacterial evolution and habitat
702 adaptation. ISME J. 15:211–227.

703 Copetti D., Búrquez A., Bustamante E., Charboneau J.L.M., Childs K.L., Eguiarte L.E., Lee S.,
704 Liu T.L., McMahon M.M., Whiteman N.K., Wing R.A., Wojciechowski M.F., Sanderson
705 M.J. 2017. Extensive gene tree discordance and hemiplasy shaped the genomes of North
706 American columnar cacti. Proc. Natl. Acad. Sci. U. S. A. 114:12003–12008.

707 DeFaveri J., Shikano T., Shimada Y., Goto A., Merilä J. 2011. Global analysis of genes involved
708 in freshwater adaptation in threespine sticklebacks (*Gasterosteus aculeatus*). Evolution.
709 65:1800–1807.

710 Degnan J.H., Rosenberg N.A. 2006a. Discordance of species trees with their most likely gene
711 trees. PLoS Genet. 2:e68.

712 Dickson B., Yashayaev I., Meincke J., Turrell B., Dye S., Holfort J. 2002. Rapid freshening of
713 the deep North Atlantic Ocean over the past four decades. Nature. 416:832–837.

714 Dittami S.M., Heesch S., Olsen J.L., Collén J. 2017. Transitions between marine and freshwater
715 environments provide new clues about the origins of multicellular plants and algae. J.
716 Phycol. 53:731–745.

717 Downey K.M., Judy K.J., Pinseel E., Alverson A.J., Lewis J.A. 2022. The dynamic response to
718 hypoosmotic stress reveals distinct stages of freshwater acclimation by a euryhaline diatom.
719 bioRxiv.:2022.06.24.497401.

720 Edelman N.B., Frandsen P.B., Miyagi M., Clavijo B., Davey J., Dikow R.B., García-Accinelli
721 G., Van Belleghem S.M., Patterson N., Neafsey D.E., Challis R., Kumar S., Moreira G.R.P.,
722 Salazar C., Chouteau M., Counterman B.A., Papa R., Blaxter M., Reed R.D., Dasmahapatra
723 K.K., Kronforst M., Joron M., Jiggins C.D., McMillan W.O., Di Palma F., Blumberg A.J.,

724 Wakeley J., Jaffe D., Mallet J. 2019. Genomic architecture and introgression shape a
725 butterfly radiation. Science. 366:594–599.

726 Edwards S.V. 2009. Is a new and general theory of molecular systematics emerging? Evolution.
727 63:1–19.

728 Elmer K.R., Meyer A. 2011. Adaptation in the age of ecological genomics: insights from
729 parallelism and convergence. Trends Ecol. Evol. 26:298–306.

730 Emms D.M., Kelly S. 2019. OrthoFinder: phylogenetic orthology inference for comparative
731 genomics. Genome Biol. 20:238.

732 Felsenstein J. 1985. Phylogenies and the Comparative Method. Am. Nat. 125:1–15.

733 Flouri T., Jiao X., Rannala B., Yang Z. 2018. Species Tree Inference with BPP Using Genomic
734 Sequences and the Multispecies Coalescent. Mol. Biol. Evol. 35:2585–2593.

735 Flouri T., Jiao X., Rannala B., Yang Z. 2020. A Bayesian Implementation of the Multispecies
736 Coalescent Model with Introgression for Phylogenomic Analysis. Mol. Biol. Evol.
737 37:1211–1223.

738 Forthman M., Braun E.L., Kimball R.T. 2022. Gene tree quality affects empirical coalescent
739 branch length estimation. Zool. Scr. 51:1–13.

740 Foster P.G. 2004. Modeling compositional heterogeneity. Syst. Biol. 53:485–495.

741 Gillung J.P., Winterton S.L., Bayless K.M., Khouri Z., Borowiec M.L., Yeates D., Kimsey L.S.,
742 Misof B., Shin S., Zhou X., Mayer C., Petersen M., Wiegmann B.M. 2018. Anchored
743 phylogenomics unravels the evolution of spider flies (Diptera, Acroceridae) and reveals

discordance between nucleotides and amino acids. Mol. Phylogenet. Evol. 128:233–245.

Gomez-Mestre I., Jovani R. 2013. A heuristic model on the role of plasticity in adaptive evolution: plasticity increases adaptation, population viability and genetic variation. Proc. Biol. Sci. 280:20131869.

Guerrero R.F., Hahn M.W. 2018. Quantifying the risk of hemiplasy in phylogenetic inference. Proc. Natl. Acad. Sci. U. S. A. 115:12787–12792.

Guillard R.R.L., Ryther J.H. 1962. Studies of marine planktonic diatoms: Guillard R. R. L. and J. H. Ryther, 1962. I. *Cyclotella nana* Hustedt, and *Detonula confervacea* (Cleve) Gran. Can J Microbiol. 8:229–240.

Hahn M.W., Nakhleh L. 2016. Irrational exuberance for resolved species trees. Evolution. 70:7–17.

Hibbins M.S., Gibson M.J., Hahn M.W. 2020. Determining the probability of hemiplasy in the presence of incomplete lineage sorting and introgression. Elife. 9.

Huang H., Knowles L.L. 2009. What is the danger of the anomaly zone for empirical phylogenetics? Syst. Biol. 58:527–536.

Hughes L.C., Ortí G., Huang Y., Sun Y., Baldwin C.C., Thompson A.W., Arcila D., Betancur-R R., Li C., Becker L., Bellora N., Zhao X., Li X., Wang M., Fang C., Xie B., Zhou Z., Huang H., Chen S., Venkatesh B., Shi Q. 2018. Comprehensive phylogeny of ray-finned fishes (Actinopterygii) based on transcriptomic and genomic data. Proc. Natl. Acad. Sci. U. S. A. 115:6249–6254.

764 Hughes L.C., Somoza G.M., Nguyen B.N., Bernot J.P., González-Castro M., Díaz de Astarloa
765 J.M., Ortí G. 2017. Transcriptomic differentiation underlying marine-to-freshwater
766 transitions in the South American silversides *Odontesthes argentinensis* and *O. bonariensis*
767 (Atheriniformes). Ecol. Evol. 7:5258–5268.

768 Jombart T., Kendall M., Almagro-Garcia J., Colijn C. 2017. treespace: Statistical exploration of
769 landscapes of phylogenetic trees. Mol. Ecol. Resour. 17:1385–1392.

770 Jones F.C., Grabherr M.G., Chan Y.F., Russell P., Mauceli E., Johnson J., Swofford R., Pirun
771 M., Zody M.C., White S., Birney E., Searle S., Schmutz J., Grimwood J., Dickson M.C.,
772 Myers R.M., Miller C.T., Summers B.R., Knecht A.K., Brady S.D., Zhang H., Pollen A.A.,
773 Howes T., Amemiya C., Broad Institute Genome Sequencing Platform & Whole Genome
774 Assembly Team, Baldwin J., Bloom T., Jaffe D.B., Nicol R., Wilkinson J., Lander E.S., Di
775 Palma F., Lindblad-Toh K., Kingsley D.M. 2012. The genomic basis of adaptive evolution
776 in threespine sticklebacks. Nature. 484:55–61.

777 Kalyaanamoorthy S., Minh B.Q., Wong T.K.F., von Haeseler A., Jermiin L.S. 2017.
778 ModelFinder: fast model selection for accurate phylogenetic estimates. Nat. Methods.
779 14:587–589.

780 Katoh K., Standley D.M. 2013. MAFFT multiple sequence alignment software version 7:
781 improvements in performance and usability. Mol. Biol. Evol. 30:772–780.

782 Kenny N.J., Plese B., Riesgo A., Itskovich V.B. 2019. Symbiosis, Selection and Novelty:
783 Freshwater Adaptation in the Unique Sponges of Lake Baikal. Mol. Biol. Evol.

784 Kent C.F., Minaei S., Harpur B.A., Zayed A. 2012. Recombination is associated with the

785 evolution of genome structure and worker behavior in honey bees. Proc. Natl. Acad. Sci. U.
786 S. A. 109:18012–18017.

787 Kirst G.O. 1990. Salinity Tolerance of Eukaryotic Marine Algae. Annu. Rev. Plant Physiol. Plant
788 Mol. Biol. 41:21–53.

789 Kirst G.O. 1996. Osmotic Adjustment in Phytoplankton and MacroAlgae. In: Kiene R.P.,
790 Visscher P.T., Keller M.D., Kirst G.O., editors. Biological and Environmental Chemistry of
791 DMSP and Related Sulfonium Compounds. Boston, MA: Springer US. p. 121–129.

792 Koester J.A., Swalwell J.E., von Dassow P., Armbrust E.V. 2010. Genome size differentiates co-
793 occurring populations of the planktonic diatom *Ditylum brightwellii* (Bacillariophyta). BMC
794 Evol. Biol. 10:1.

795 Kubatko L.S., Degnan J.H. 2007. Inconsistency of phylogenetic estimates from concatenated
796 data under coalescence. Syst. Biol. 56:17–24.

797 Lartillot N. 2013. Phylogenetic patterns of GC-biased gene conversion in placental mammals and
798 the evolutionary dynamics of recombination landscapes. Mol. Biol. Evol. 30:489–502.

799 Lartillot N., Philippe H. 2004. A Bayesian mixture model for across-site heterogeneities in the
800 amino-acid replacement process. Mol. Biol. Evol. 21:1095–1109.

801 L E E C.E., Downey K., Colby R.S., Freire C.A., Nichols S., Burgess M.N., Judy K.J. 2022.
802 Recognizing salinity threats in the climate crisis. Integr. Comp. Biol.

803 Linkem C.W., Minin V.N., Leaché A.D. 2016. Detecting the Anomaly Zone in Species Trees
804 and Evidence for a Misleading Signal in Higher-Level Skink Phylogeny (Squamata:

805 Scincidae). Syst. Biol. 65:465–477.

806 Liu L., Wu S., Yu L. 2015. Coalescent methods for estimating species trees from phylogenomic
807 data. J. Syst. Evol. 53:380–390.

808 Logares R., Bråte J., Bertilsson S., Clasen J.L., Shalchian-Tabrizi K., Rengefors K. 2009.
809 Infrequent marine-freshwater transitions in the microbial world. Trends Microbiol. 17:414–
810 422.

811 López-Maury L., Marguerat S., Bähler J. 2008. Tuning gene expression to changing
812 environments: from rapid responses to evolutionary adaptation. Nat. Rev. Genet. 9:583–
813 593.

814 Lozupone C.A., Knight R. 2007. Global patterns in bacterial diversity. Proc. Natl. Acad. Sci. U.
815 S. A. 104:11436–11440.

816 Maddison W.P. 1997. Gene Trees in Species Trees. Syst. Biol. 46:523–536.

817 Mallet J., Besansky N., Hahn M.W. 2016. How reticulated are species? Bioessays. 38:140–149.

818 Mann D.G. 1999. Crossing the Rubicon : the effectiveness of the marine/freshwater interface as
819 a barrier to the migration of diatom germplasm. Proceedings of the 14th International
820 Diatom Symposium, Koenigstein, 1999.:1–21.

821 McCairns R.J.S., Bernatchez L. 2010. Adaptive divergence between freshwater and marine
822 sticklebacks: insights into the role of phenotypic plasticity from an integrated analysis of
823 candidate gene expression. Evolution. 64:1029–1047.

824 McInerney J.O. 1998. GCUA: general codon usage analysis. Bioinformatics. 14:372–373.

825 Mendes F.K., Hahn Y., Hahn M.W. 2016. Gene Tree Discordance Can Generate Patterns of
826 Diminishing Convergence over Time. Mol. Biol. Evol. 33:3299–3307.

827 Minh B.Q., Hahn M.W., Lanfear R. 2020a. New Methods to Calculate Concordance Factors for
828 Phylogenomic Datasets. Mol. Biol. Evol. 37:2727–2733.

829 Minh B.Q., Nguyen M.A.T., von Haeseler A. 2013. Ultrafast Approximation for Phylogenetic
830 Bootstrap. Mol. Biol. Evol. 30:1188–1195.

831 Minh B.Q., Schmidt H.A., Chernomor O., Schrempf D., Woodhams M.D., von Haeseler A.,
832 Lanfear R. 2020b. IQ-TREE 2: New Models and Efficient Methods for Phylogenetic
833 Inference in the Genomic Era. Mol. Biol. Evol. 37:1530–1534.

834 Mirarab S. 2017. Phylogenomics: Constrained gene tree inference. Nat Ecol Evol. 1:56.

835 Mirarab S., Reaz R., Bayzid M.S., Zimmermann T., Swenson M.S., Warnow T. 2014. ASTRAL:
836 genome-scale coalescent-based species tree estimation. Bioinformatics. 30:i541–i548.

837 Mitterboeck T.F., Chen A.Y., Zaheer O.A., Ma E.Y.T., Adamowicz S.J. 2016. Do saline taxa
838 evolve faster? Comparing relative rates of molecular evolution between freshwater and
839 marine eukaryotes. Evolution. 70:1960–1978.

840 Molloy E.K., Warnow T. 2018. To Include or Not to Include: The Impact of Gene Filtering on
841 Species Tree Estimation Methods. Syst. Biol. 67:285–303.

842 Morales-Briones D.F., Kadereit G., Tefarikis D.T., Moore M.J., Smith S.A., Brockington S.F.,
843 Timoneda A., Yim W.C., Cushman J.C., Yang Y. 2020. Disentangling Sources of Gene
844 Tree Discordance in Phylogenomic Data Sets: Testing Ancient Hybridizations in

Amaranthaceae s.l. Syst. Biol. 70:219–235.

Nakov T., Beaulieu J.M., Alverson A.J. 2018. Accelerated diversification is related to life history and locomotion in a hyperdiverse lineage of microbial eukaryotes (Diatoms, Bacillariophyta). New Phytol. 219:462–473.

Nakov T., Beaulieu J.M., Alverson A.J. 2019. Diatoms diversify and turn over faster in freshwater than marine environments. Evolution. 73:2497–2511.

Nakov T., Judy K.J., Downey K.M., Ruck E.C., Alverson A.J. 2020. Transcriptional Response of Osmolyte Synthetic Pathways and Membrane Transporters in a Euryhaline Diatom During Long-term Acclimation to a Salinity Gradient. J. Phycol. 56:1712–1728.

Naser-Khdour S., Minh B.Q., Zhang W., Stone E.A., Lanfear R. 2019. The Prevalence and Impact of Model Violations in Phylogenetic Analysis. Genome Biol. Evol. 11:3341–3352.

Nawaly H., Tsuji Y., Matsuda Y. 2020. Rapid and precise genome editing in a marine diatom, *Thalassiosira pseudonana* by Cas9 nickase (D10A). Algal Research. 47:101855.

Nesi N., Tsagkogeorga G., Tsang S.M., Nicolas V., Lalis A., Scanlon A.T., Riesle-Sbarbaro S.A., Wiantoro S., Hitch A.T., Juste J., Pinzari C.A., Bonaccorso F.J., Todd C.M., Lim B.K., Simmons N.B., McGowen M.R., Rossiter S.J. 2021. Interrogating Phylogenetic Discordance Resolves Deep Splits in the Rapid Radiation of Old World Fruit Bats (Chiroptera: Pteropodidae). Syst. Biol. 70:1077–1089.

Parks M.B., Nakov T., Ruck E.C., Wickett N.J., Alverson A.J. 2018. Phylogenomics reveals an extensive history of genome duplication in diatoms (Bacillariophyta). Am. J. Bot. 105:330–

347.

Paver S.F., Muratore D., Newton R.J., Coleman M.L. 2018. Reevaluating the Salty Divide: Phylogenetic Specificity of Transitions between Marine and Freshwater Systems. mSystems. 3.

Pease J.B., Brown J.W., Walker J.F., Hinchliff C.E., Smith S.A. 2018. Quartet Sampling distinguishes lack of support from conflicting support in the green plant tree of life. Am. J. Bot. 105:385–403.

Pease J.B., Hahn M.W. 2013. More accurate phylogenies inferred from low-recombination regions in the presence of incomplete lineage sorting. Evolution. 67:2376–2384.

Philippe H., Brinkmann H., Lavrov D.V., Littlewood D.T.J., Manuel M., Wörheide G., Baurain D. 2011. Resolving difficult phylogenetic questions: why more sequences are not enough. PLoS Biol. 9:e1000602.

Phillips M.J., Penny D. 2003. The root of the mammalian tree inferred from whole mitochondrial genomes. Mol. Phylogenet. Evol. 28:171–185.

Pinseel E., Nakov T., Van den Berge K., Downey K.M., Judy K.J., Kourtchenko O., Kremp A., Ruck E.C., Sjöqvist C., Töpel M., Godhe A., Alverson A.J. 2022. Strain-specific transcriptional responses overshadow salinity effects in a marine diatom sampled along the Baltic Sea salinity cline. ISME J.

Prabha R., Singh D.P., Sinha S., Ahmad K., Rai A. 2017. Genome-wide comparative analysis of codon usage bias and codon context patterns among cyanobacterial genomes. Mar.

885 Genomics. 32:31–39.

886 Price M.N., Dehal P.S., Arkin A.P. 2010. FastTree 2--approximately maximum-likelihood trees
887 for large alignments. PLoS One. 5:e9490.

888 Regier J.C., Shultz J.W., Zwick A., Hussey A., Ball B., Wetzer R., Martin J.W., Cunningham
889 C.W. 2010. Arthropod relationships revealed by phylogenomic analysis of nuclear protein-
890 coding sequences. Nature. 463:1079–1083.

891 Reis M. dos, Yang Z. 2011. Approximate Likelihood Calculation on a Phylogeny for Bayesian
892 Estimation of Divergence Times. Mol. Biol. Evol. 28:2161–2172.

893 Roberts W.R., Downey K.M., Ruck E.C., Traller J.C., Alverson A.J. 2020. Improved Reference
894 Genome for *Cyclotella cryptica* CCMP332, a Model for Cell Wall Morphogenesis, Salinity
895 Adaptation, and Lipid Production in Diatoms (Bacillariophyta). G3 . 10:2965–2974.

896 [dataset]* Roberts W.R., Ruck E.C., Downey K.M., Alverson A.J. 2022. Resolving marine–
897 freshwater transitions by diatoms through a fog of discordance and hemiplasy. Dryad.
898 http://dx.doi.org/10.5061/dryad.[NNNN].

899 Roch S., Warnow T. 2015. On the Robustness to Gene Tree Estimation Error (or lack thereof) of
900 Coalescent-Based Species Tree Methods. Syst. Biol. 64:663–676.

901 Rogers R.L., Grizzard S.L., Titus-McQuillan J.E., Bockrath K., Patel S., Wares J.P., Garner J.T.,
902 Moore C.C. 2021. Gene family amplification facilitates adaptation in freshwater unionid
903 bivalve Megalonaias nervosa. Mol. Ecol. 30:1155–1173.

904 Roller M., Lucić V., Nagy I., Perica T., Vlahovicek K. 2013. Environmental shaping of codon

usage and functional adaptation across microbial communities. Nucleic Acids Res. 41:8842–8852.

Rosenberg N.A. 2003. The shapes of neutral gene genealogies in two species: probabilities of monophyly, paraphyly, and polyphyly in a coalescent model. Evolution. 57:1465–1477.

Rota-Stabelli O., Lartillot N., Philippe H., Pisani D. 2012. Serine Codon-Usage Bias in Deep Phylogenomics: Pancrustacean Relationships as a Case Study. Syst. Biol. 62:121–133.

Salichos L., Stamatakis A., Rokas A. 2014. Novel information theory-based measures for quantifying incongruence among phylogenetic trees. Mol. Biol. Evol. 31:1261–1271.

Sanderson M.J., Wojciechowski M.F., Hu J.M., Khan T.S., Brady S.G. 2000. Error, bias, and long-branch attraction in data for two chloroplast photosystem genes in seed plants. Mol. Biol. Evol. 17:782–797.

Sayyari E., Mirarab S. 2016. Fast Coalescent-Based Computation of Local Branch Support from Quartet Frequencies. Mol. Biol. Evol. 33:1654–1668.

Sayyari E., Mirarab S. 2018. Testing for Polytomies in Phylogenetic Species Trees Using Quartet Frequencies. Genes . 9.

Shimodaira H. 2002. An approximately unbiased test of phylogenetic tree selection. Syst. Biol. 51:492–508.

Simmons M.P., Gatesy J. 2021. Collapsing dubiously resolved gene-tree branches in phylogenomic coalescent analyses. Mol. Phylogenet. Evol. 158:107092.

Simmons M.P., Ochoterena H., Freudenstein J.V. 2002. Amino acid vs. nucleotide characters:

challenging preconceived notions. Mol. Phylogenet. Evol. 24:78–90.

Skinner R.K., Dietrich C.H., Walden K.K.O., Gordon E., Sweet A.D., Podsiadlowski L., Petersen M., Simon C., Takiya D.M., Johnson K.P. 2020. Phylogenomics of Auchenorrhyncha (Insecta: Hemiptera) using transcriptomes: examining controversial relationships via degeneracy coding and interrogation of gene conflict. Syst. Entomol. 45:85–113.

Slatkin M., Pollack J.L. 2008. Subdivision in an ancestral species creates asymmetry in gene trees. Mol. Biol. Evol. 25:2241–2246.

Smith S.A., Brown J.W., Walker J.F. 2018. So many genes, so little time: A practical approach to divergence-time estimation in the genomic era. PLoS One. 13:e0197433.

Smith S.A., Moore M.J., Brown J.W., Yang Y. 2015. Analysis of phylogenomic datasets reveals conflict, concordance, and gene duplications with examples from animals and plants. BMC Evol. Biol. 15:150.

Steenwyk J.L., Buida T.J., Labella A.L., Li Y., Shen X.-X., Rokas A. 2021. PhyKIT: a broadly applicable UNIX shell toolkit for processing and analyzing phylogenomic data. Bioinformatics.

Stern D.B., Anderson N.W., Diaz J.A., Lee C.E. 2022. Genome-wide signatures of synergistic epistasis during parallel adaptation in a Baltic Sea copepod. Nat. Commun. 13:4024.

Storz J.F. 2016. Causes of molecular convergence and parallelism in protein evolution. Nat. Rev. Genet. 17:239–250.

945 Suyama M., Torrents D., Bork P. 2006. PAL2NAL: robust conversion of protein sequence
946 alignments into the corresponding codon alignments. Nucleic Acids Res. 34:W609–W612.

947 Tanaka T., Maeda Y., Veluchamy A., Tanaka M., Abida H., Maréchal E., Bowler C., Muto M.,
948 Sunaga Y., Tanaka M., Yoshino T., Taniguchi T., Fukuda Y., Nemoto M., Matsumoto M.,
949 Wong P.S., Aburatani S., Fujibuchi W. 2015. Oil accumulation by the oleaginous diatom
950 *Fistulifera solaris* as revealed by the genome and transcriptome. Plant Cell. 27:162–176.

951 Tea Y.-K., Xu X., DiBattista J.D., Lo N., Cowman P.F., Ho S.Y.W. 2021. Phylogenomic
952 Analysis of Concatenated Ultraconserved Elements Reveals the Recent Evolutionary
953 Radiation of the Fairy Wrasses (Teleostei: Labridae: *Cirrhilabrus*). Syst. Biol. 71:1–12.

954 Tedesco P.A., Paradis E., Lévêque C., Hugueny B. 2017. Explaining global-scale diversification
955 patterns in actinopterygian fishes. J. Biogeogr. 44:773–783.

956 Terekhanova N.V., Barmintseva A.E., Kondrashov A.S., Bazykin G.A., Mugue N.S. 2019.
957 Architecture of Parallel Adaptation in Ten Lacustrine Threespine Stickleback Populations
958 from the White Sea Area. Genome Biol. Evol. 11:2605–2618.

959 Theriot E.C., Fritz S.C., Whitlock C., Conley D.J. 2006. Late Quaternary rapid morphological
960 evolution of an endemic diatom in Yellowstone Lake, Wyoming. Paleobiology. 32:38–54.

961 Theriot E., Stoermer E., Håkansson H. 1987. Taxonomic interpretation of the rimoportula of
962 freshwater genera in the centric diatom family Thalassiosiraceae. Diatom Res. 2:251–265.

963 Townsend J.P., López-Giráldez F., Friedman R. 2008. The phylogenetic informativeness of
964 nucleotide and amino acid sequences for reconstructing the vertebrate tree. J. Mol. Evol.

965 67:437–447.

966 Tricou T., Tannier E., de Vienne D.M. 2022. Ghost Lineages Highly Influence the Interpretation
967 of Introgression Tests. Syst. Biol.

968 Vanderpool D., Minh B.Q., Lanfear R., Hughes D., Murali S., Harris R.A., Raveendran M.,
969 Muzny D.M., Hibbins M.S., Williamson R.J., Gibbs R.A., Worley K.C., Rogers J., Hahn
970 M.W. 2020. Primate phylogenomics uncovers multiple rapid radiations and ancient
971 interspecific introgression. PLoS Biol. 18:e3000954.

972 Villar H.O., Kauvar L.M. 1994. Amino acid preferences at protein binding sites. FEBS Lett.
973 349:125–130.

974 Vizueta J., Macías-Hernández N., Arnedo M.A., Rozas J., Sánchez-Gracia A. 2019. Chance and
975 predictability in evolution: The genomic basis of convergent dietary specializations in an
976 adaptive radiation. Mol. Ecol. 28:4028–4045.

977 Wang H.-C., Minh B.Q., Susko E., Roger A.J. 2018. Modeling Site Heterogeneity with Posterior
978 Mean Site Frequency Profiles Accelerates Accurate Phylogenomic Estimation. Syst. Biol.
979 67:216–235.

980 Wray G.A. 2007. The evolutionary significance of cis-regulatory mutations. Nat. Rev. Genet.
981 8:206–216.

982 Wu M., Kostyun J.L., Hahn M.W., Moyle L.C. 2018. Dissecting the basis of novel trait evolution
983 in a radiation with widespread phylogenetic discordance. Mol. Ecol.

984 Xi Z., Liu L., Davis C.C. 2015. Genes with minimal phylogenetic information are problematic

985 for coalescent analyses when gene tree estimation is biased. Mol. Phylogenet. Evol. 92:63–
986 71.

987 Yang Y., Smith S.A. 2014. Orthology inference in nonmodel organisms using transcriptomes
988 and low-coverage genomes: improving accuracy and matrix occupancy for phylogenomics.
989 Mol. Biol. Evol. 31:3081–3092.

990 Yang Z. 2007. PAML 4: phylogenetic analysis by maximum likelihood. Mol. Biol. Evol.
991 24:1586–1591.

992 Youssef N., Susko E., Roger A.J., Bielawski J.P. 2021. Shifts in amino acid preferences as
993 proteins evolve: A synthesis of experimental and theoretical work. Protein Sci. 30:2009–
994 2028.

995 Yuan Z., Liu S., Zhou T., Tian C., Bao L., Dunham R., Liu Z. 2018. Comparative genome
996 analysis of 52 fish species suggests differential associations of repetitive elements with their
997 living aquatic environments. BMC Genomics. 19:141.

998 Zhang C., Rabiee M., Sayyari E., Mirarab S. 2018. ASTRAL-III: polynomial time species tree
999 reconstruction from partially resolved gene trees. BMC Bioinformatics. 19:153.

1000 Zou Z., Zhang J. 2015. Are Convergent and Parallel Amino Acid Substitutions in Protein
1001 Evolution More Prevalent Than Neutral Expectations? Mol. Biol. Evol. 32:2085–2096.

1002 Zwick A., Regier J.C., Zwickl D.J. 2012. Resolving discrepancy between nucleotides and amino
1003 acids in deep-level arthropod phylogenomics: differentiating serine codons in 21-amino-
1004 acid models. PLoS One. 7:e47450.

1005 FIGURE LEGENDS

1006 Figure 1. Phylogram based on maximum likelihood analysis of amino acids using the posterior
1007 mean site frequency (PMSF) model and a dataset of 488 loci with the highest proportions of taxa
1008 and informative sites ("AA-top-PI-top-Taxa" dataset; Table 1). Backbone nodes of the
1009 *Thalassiosira* grade are indicated by the letters A–E. All branches had bootstrap support (BS)
1010 values of 100 except for those with black circles which had BS = 90. Pie charts on backbone
1011 nodes show the proportion of gene trees that support the clade (gCF), the proportion that support
1012 both discordant topologies (gDF1, gDF2), and the proportion that are discordant due to
1013 polyphyly (gDFP). The size of the pie charts is only for aesthetics.
1014
1015 Figure 2. **a)** Phylogenetic hypotheses of the *Thalassiosira* grade inferred using concatenation and
1016 summary methods on the amino acid (AA), codon positions 1 and 2 (CDS12), and recoded
1017 codon (DEGEN) datasets. Nodes are labeled with the percentage of amino acid sites concordant
1018 with the branch (site concordance factor). The principal clade of interest, the freshwater
1019 cyclostephanoids, is colored orange and labeled 'FW'. The four focal clades of marine
1020 *Thalassiosira* and allies are labeled I–IV. Below, results of gene genealogy interrogation tests of
1021 alternative hypotheses of relationships within the *Thalassiosira* grade. These tests used datasets
1022 filtered to include only the top 25% of orthologs based on the percentage of parsimony
1023 informative sites (top-PI) for **b)** amino acids, **c)** codon positions 1 and 2, and **d)** recoded codons.
1024 Lines correspond to the cumulative number of genes (x-axis) supporting topology hypotheses
1025 with the highest probability and their *P* values (y-axis) from the Approximately Unbiased (AU)
1026 topology tests. Values above the dashed line indicate topological hypotheses that are
1027 significantly better than the alternatives ($P < 0.05$). For example, the green line in (b) shows that

there were a total of 88 genes that best supported topology 3, while only four of those genes were above the dotted line and were significantly better supported than the other four alternative topologies.

Figure 3. **a)** Divergence times and ancestral state reconstruction of marine and freshwater habitat in the Thalassiosirales. Conspecific taxa were removed prior to ancestral state reconstruction, leaving one tip per species. Tip labels are colored according to their habitat (blue=freshwater, orange=euryhaline, grey=marine). Pie charts denote the probability of each node reconstructed as either marine (grey) or freshwater (blue) using parameters estimated from the HiSSE CID–4 model. Euryhaline taxa were coded as marine for the purposes of ancestral state reconstruction. Divergence times for the full set of taxa can be found in Supplementary Fig. S9. **b)** Hemiplasy Risk Factors (HRF) on internal branches show increased values on most short internal branches, demonstrating an increased potential for hemiplasy to influence trait reconstruction. Branch lengths in coalescent units were inferred using ASTRAL.

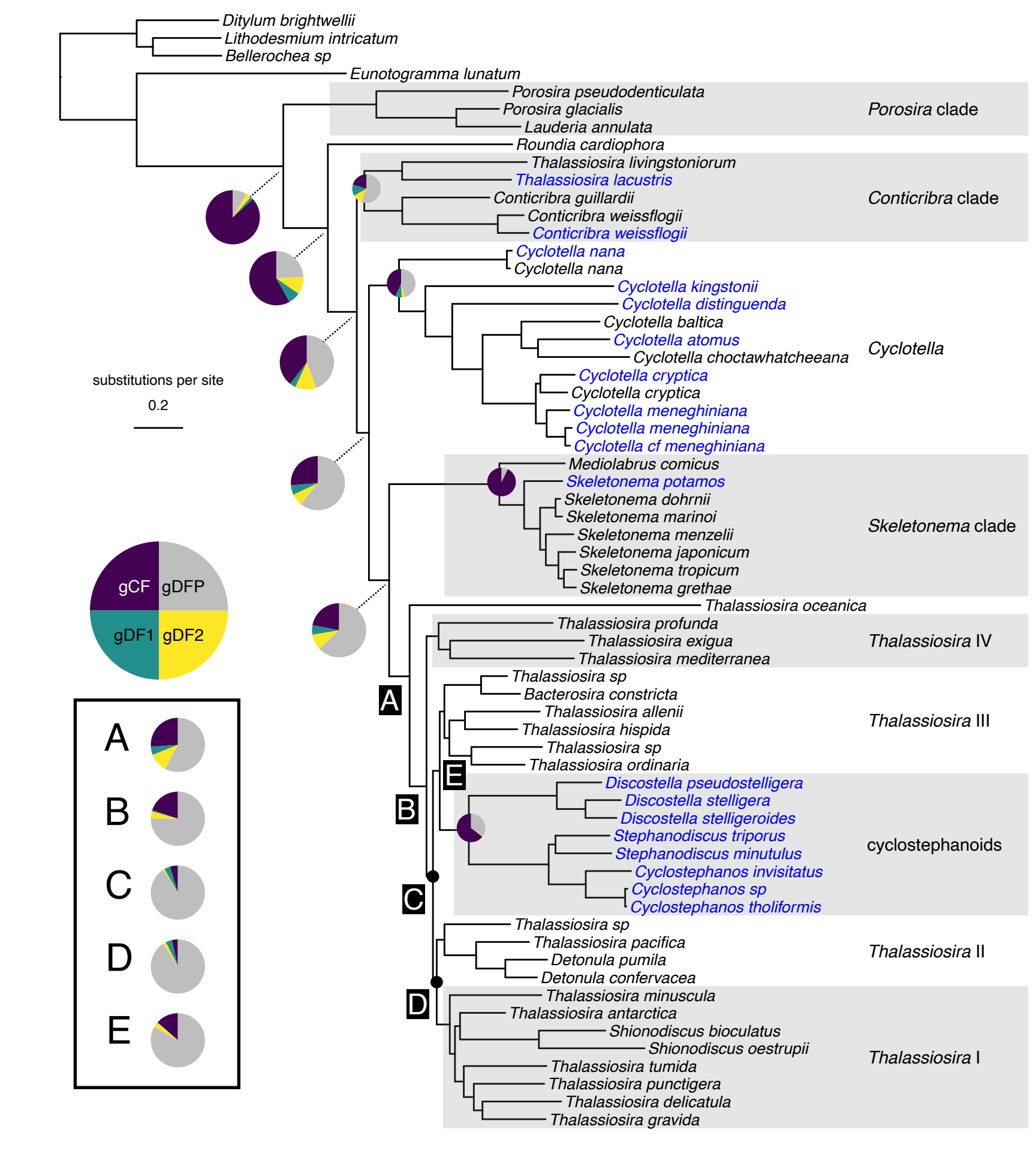
Ditylum brightwellii
Lithodesmium intricatum
Bellerochea sp
Eunotogramma lunatum
Porosira pseudodenticulata
Porosira glacialis
Lauderia annulata
Porosira clade
Roundia cardiophora
Thalassiosira livingstoniorum
Thalassiosira lacustris
Conticribra guillardii
Conticribra weissflogii
Conticribra weissflogii
Conticribra clade
Cyclotella nana
Cyclotella nana
Cyclotella kingstonii
Cyclotella distinguenda
Cyclotella baltica
Cyclotella atomus
Cyclotella choctawhatcheeana
Cyclotella cryptica
Cyclotella cryptica
Cyclotella meneghiniana
Cyclotella meneghiniana
Cyclotella cf meneghiniana
Cyclotella
substitutions per site
0.2
Mediolabrus comicus
Skeletonema potamos
Skeletonema dohrnii
Skeletonema marinoi
Skeletonema menzelii
Skeletonema japonicum
Skeletonema tropicum
Skeletonema grethae
Skeletonema clade
gCF
gDFP
gDF1
gDF2
Thalassiosira oceanica
Thalassiosira profunda
Thalassiosira exigua
Thalassiosira mediterranea
Thalassiosira IV
A
Thalassiosira sp
Bacterosira constricta
Thalassiosira allenii
Thalassiosira hispida
Thalassiosira sp
Thalassiosira ordinaria
Thalassiosira III
E
B
Discostella pseudostelligera
Discostella stelligera
Discostella stelligeroides
Stephanodiscus triporus
Stephanodiscus minutulus
Cyclostephanos invisitatus
Cyclostephanos sp
Cyclostephanos tholiformis
cyclostephanoids
C
Thalassiosira sp
Thalassiosira pacifica
Detonula pumila
Detonula confervacea
Thalassiosira II
D
Thalassiosira minuscula
Thalassiosira antarctica
Shionodiscus bioculatus
Shionodiscus oestrupii
Thalassiosira tumida
Thalassiosira punctigera
Thalassiosira delicatula
Thalassiosira gravida
Thalassiosira I
A
B
C
D
E

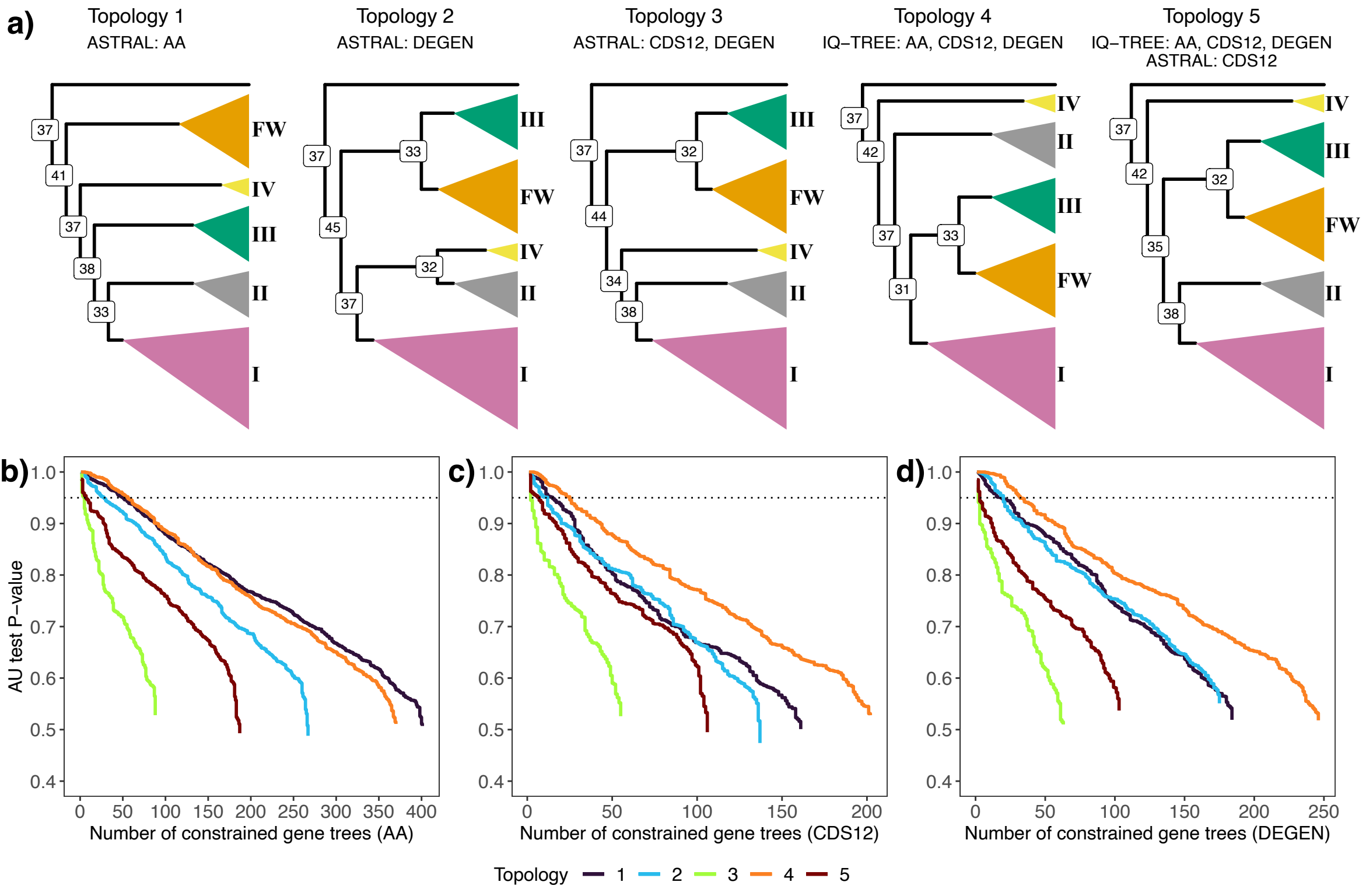
a)
Topology 1
ASTRAL: AA
Topology 2
ASTRAL: DEGEN
Topology 3
ASTRAL: CDS12, DEGEN
Topology 4
IQ–TREE: AA, CDS12, DEGEN
Topology 5
IQ–TREE: AA, CDS12, DEGEN
ASTRAL: CDS12
FW
IV
III
II
I
b)
c)
d)
AU test P–value
Number of constrained gene trees (AA)
Number of constrained gene trees (CDS12)
Number of constrained gene trees (DEGEN)
Topology 1 2 3 4 5

a)

b)

Porosira pseudodenticulata
Porosira glacialis
Lauderia annulata
Roundia cardiophora
Thalassiosira livingstoniorum
Thalassiosira lacustris
Conticribra guillardii
Conticribra weissflogii
Cyclotella nana
Cyclotella kingstonii
Cyclotella distinguenda
Cyclotella cryptica
Cyclotella meneghiniana
Cyclotella baltica
Cyclotella choctawhatcheeana
Cyclotella atomus
Mediolabrus comicus
Skeletonema potamos
Skeletonema dohrnii
Skeletonema marinoi
Skeletonema menzelii
Skeletonema japonicum
Skeletonema tropicum
Skeletonema grethae
Thalassiosira oceanica
Thalassiosira profunda
Thalassiosira exigua
Thalassiosira mediterranea
Thalassiosira sp
Bacterosira constricta
Thalassiosira sp
Thalassiosira ordinaria
Thalassiosira hispida
Thalassiosira allenii
Discostella pseudostelligera
Discostella stelligera
Discostella stelligeroides
Stephanodiscus triporus
Stephanodiscus minutulus
Cyclostephanos invisitatus
Cyclostephanos tholiformis
Thalassiosira sp
Thalassiosira pacifica
Detonula pumila
Detonula confervacea
Thalassiosira minuscula
Thalassiosira antarctica
Shionodiscus bioculatus
Shionodiscus oestrupii
Thalassiosira tumida
Thalassiosira punctigera
Thalassiosira delicatula
Thalassiosira gravida

freshwater
euryhaline
marine

100 80 60 40 20 0
Million Years Ago (Ma)

Hemiplasy Risk Factor
1.00
0.75
0.50
0.25
0.00

coalescent units
1